UNIVERSITETET I AGDER

Condition Monitoring of Steel Wire Ropes

DANIEL ÅRRESTAD STAVE

PROFESSOR GEIR GRASMO
Associate Professor Dmitry Vysochinskiy
Senior Researcher Rune Schlanbusch (Teknova AS)

University of Agder, 2018
Faculty of Engineering and Science
Department of Engineering Sciences

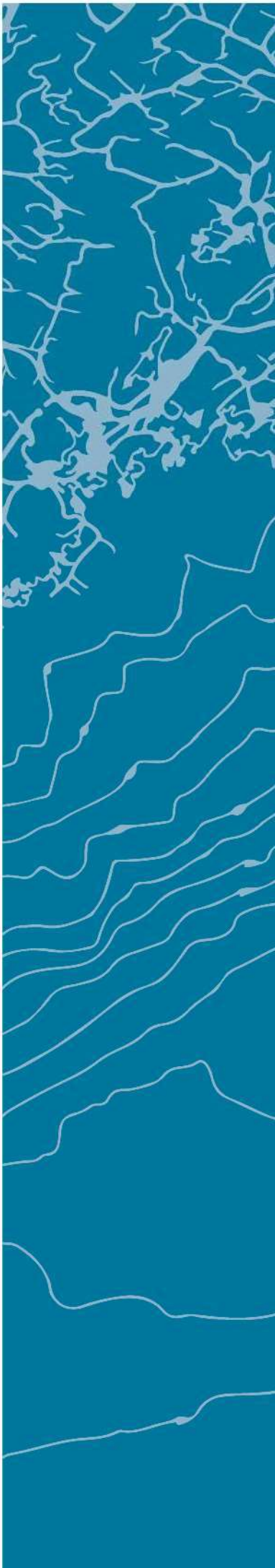

This page was intentionally left blank

Abstract

By utilising the measurements from a commercial acoustic emission sensor system, magnetic tester and a camera system, conducted during four separate simple bending fatigue tests of steel wire ropes (SWR), several measurable quantities of the SWR which indicate deterioration were identified. Based on the measurements of a commercial acoustic emission sensor system of one of the tests in this thesis, the fatigue process of a SWRs in a simple bending test is three-phase, with a relatively long first- and second phase, showing little- and steady increase in activity, respectively, followed by a shorter phase with a ramp up of activity. This three-phase process was recognised in the three other simple bending tests through the processed measurements of a magnetic tester. For the first time, changes in the lay length of a SWR were detected using a camera system. Diameter measurements using the same camera system were unsuccessful. For one of the SWR tested, a total of ten completely ruptured strands were counted after the SWR had been discarded. However, none of these strands was located in the outer layer of the wire, thus, with the ISO 4309 recommended assessment method for fractured strand(s) being visual inspection [5, p. 11], none of them would have been detected, which is contradictory to ISO 4309's recommendation on discarding the SWR immediately if only one fractured strand is identified [5, p. 19]. A short video of the thesis is posted online and can be accessed through: https://youtu.be/4O06OYLnGug

Preface

This thesis concludes my Master of Science education in Mechatronics at the University of Agder, performed throughout spring 2018, at the Department of Engineering Sciences, in collaboration with the research centre Teknova AS.

I would like to use this opportunity to thank my two supervisors at the University of Agder; Professor Geir Grasmo and Associate Professor Dmitry Vysochinskiy, and my supervisor at Teknova; Senior Researcher Rune Schlanbusch. Without their guidance, shared knowledge and support, the outcome would have looked much different, and I am truly grateful for the time and effort they have invested in this thesis. I would also like to thank Shaun Falconer, PhD student at the University of Agder, Benyamin Akdemir, Technician at Teknova AS, Boyan Yuan, senior Researcher at Teknova AS, and Morten Kollerup Bak, Technical Manager at Mechatronics Innovation Lab, for helping me in various ways.

With the help of these people, and the support from my family, friends and girlfriend, this thesis has been an enjoyable experience.

14th of May 2018, Grimstad, Norway.

Contents

List of Figures

List of Tables

List of Symbols

Latin letters

Symbol	Description	Unit
A_c	Area of calibration rod	mm^2
a_0	Coefficient of Equation (2.2)	$-$
a_1	Coefficient of Equation (2.2)	$-$
a_2	Coefficient of Equation (2.2)	$-$
a_3	Coefficient of Equation (2.2)	$-$
b_0	Coefficient of Equation (2.7)	$-$
b_1	Coefficient of Equation (2.4) and (2.7)	$-$
b_2	Coefficient of Equation (2.7)	$-$
b_3	Coefficient of Equation (2.4) and (2.7)	$-$
c	Coefficient of Equation (2.3) and (2.4)	$-$
D	Pitch diameter of sheave with steel wire rope	mm
d	Wire diameter	mm
d_w	Measured wire diameter	mm
f_C	Endurance factor for rope core	$-$
f_d	Endurance factor for rope diameter	$-$
f_L	Endurance factor for bending length	$-$
h_w	lay length	mm
L_{ma}	Loss of metallic area	mm^2
l	bending length	mm
$lg\ x$	Natural logarithm of 10, $lg\ x = log_{10}\ x$	
N	Number of cycles	$-$
N_{1770}	Number of cycles of a wire with $R_0 = 1700\ N/mm^2$	$-$
R_0	Nominal rope strength	N/mm^2
r	Groove radius	mm
S	Tensile force applied to wire, also known as line pull	N
S_{1770}	Tensile force applied to a wire with $R_0 = 1700\ N/mm^2$	N
T_R	Rope temperature	^oC
U_h	Measured voltage of the steel wire rope by the magnetic tester	mV
U_{hc}	Measured voltage of the calibration rod by the magnetic tester	mV

List of Symbols (continuing)

Greek letters

Symbol	Description	Unit
γ	Groove angle	^{o}
θ	Lateral deflection angle	^{o}
μ	Dynamic viscosity of lubricant (tested at plate at 130^oC)	$Pa \cdot s$
φ_D	Deflecting angle	^{o}

Abbreviations

ABS	Absolute
AE	Acoustic Emission
ASL	Average Signal Level
BNC	Bayonet Neill–Concelman
CBOS	Cyclic Bend Over Sheave
CM	Condition Monitoring
DAQ	Data Aquisition
FPS	Frames Per Second
HDT	Hit Definition Time
HLT	Hit Lockout Time
LBW	Locations of Broken Wires
LED	Light-emitting Diode
LF	Local Fault
LMA	Local Magnetic Area
MIL	Mechatronics Innovation Lab
NBW	Number of Broken Wires
NDT	Non Destructive Testing
OIPEEC	International Organization for the Study of Ropes
PCB	Processing Board
PCI	Peripheral Component Interconnect
PDT	Peak Definition Time
RMS	Root Mean Square
SMRT	Stuttgart Magnetic Rope Tester
SPS	Samples Per Second
SMA	SubMiniature version A
SWR	Steel Wire Rope
UIA	University of Agder
USB	Universal Serial Bus
WSC	Wire Strand Core

Chapter 1

Introduction

Oberbergrat Wilhelm August Julius, a German engineer and mining administrator, invented the SWR in 1834 [1, p. 1]. Today, it's used in a wide range of industries, including, but not limited to, mining, cranes, cableways, shipping and offshore applications. The SWR used in the offshore oil and gas industry are subjected to extreme loading situations and harsh environments, with deep-sea water applications reaching depths of 3000 m. Their strength and quality requirements are tough, which reflects in their cost. Obviously, it's desirable to use the SWR as long as possible without having any accidents. To apply such a philosophy in industrial applications an appropriate discard criterion based on the SWR's current condition is needed. The most common discard criterion is the number of visible broken wires [2], however, manually counting the number of broken wires in a long SWR is cumbersome, unpractical, and prone to human error. By describing the condition of a SWR using quantifiable data obtained from commercially available apparatus, the counting process could be automated. Additionally, if the equipment could measure more of the SWRs features which are relevant regarding deterioration, its condition can be described more elegantly. A wire is discarded based on its condition. Thus, more information about its condition would result in more confidence in the decision of discarding it. ISO 4309, a worldwide standard for evaluating SWR [3, p. 2], suggests six discard criteria based on individual features, as well as a combined criterion taking three features into account. If the discard criterion could be improved, the lifetime of a SWR could be extended if its condition allowed for it, thus, decreasing cost, alternatively, shorten it if its condition suggests so, therefore, increasing safety.

1.1 Objective

The objective of this research is to identify measurable quantities of the SWR during a simple bending test which indicate deterioration, that is the progress of gradually becoming worse, and to eventually develop a condition monitoring (CM) model for SWRs. Such a model has the potential of bridging the gap between the SWR's current condition and fatigue life, thus, enabling determination of the remaining number of cycles based on its current condition.

1.2 Scope

The scope of this thesis is to identify measurable quantities and features of the SWR, which indicate deterioration, during a simple bending fatigue test, by utilising the data obtained by the use of a magnetic tester, an acoustic emission sensor- and a camera system.

Chapter 2

Theory

In this chapter, the central theory utilised in this thesis is presented. Starting with the terminology, common modes of deterioration, and the ISO standard's discard criteria for SWRs. Further, an introduction to fatigue is given, followed by a more in-depth study of fatigue of SWRs with emphasis on Feyrer's equation. Lastly, the theory behind the condition monitoring technologies is presented.

2.1 Steel wire ropes

SWRs consist of strands which are twisted around a core. A strand consists of steel wires, which, once again, are twisted around a centre wire or another core, as illustrated in Figure 2.1. An important property of a strand is its lay length h_w, i.e. the length measured along the rope for which a wire completes a turn around the centre wire, also illustrated in Figure 2.1. Similarly, the lay length of a SWR is the length measured along the rope for which a strand completes a turn around the core. The lay length of a SWR can be calculated by [1, p. 24]

$$h_w = \frac{\pi d_w}{tan(\alpha)} \tag{2.1}$$

where α is the angle between the longitudinal axis of the stand and SWR, as shown in Figure 2.1.

A core consists of either a strand itself or a fibrous or deformable element [4, p. 1157]. The cross-section of one of the SWRs tested in this thesis is presented in Figure 2.2. This SWR has 35 strands, which each consists of 7 wires, and the core itself consists of a stand, thus, by definition of [1, p. 31], (the core) is classified as a wire strand core (WSC).

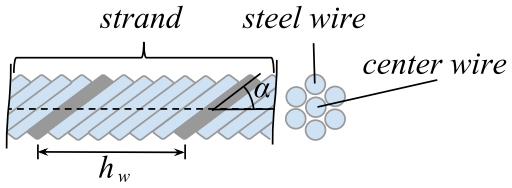

Figure 2.1: Basic terminology of a SWR, h_w denotes its lay length and α is the angle between the wires- and the strands longitudinal axis, alternatively the angle between the strands- and SWRs longitudinal axis

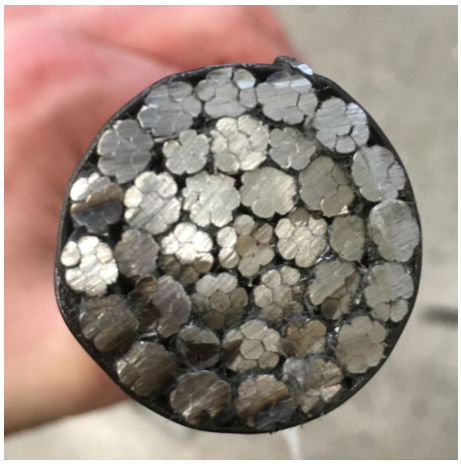

Figure 2.2: Cross-section of one the SWR tested in this thesis

2.1.1 Condition of steel wire ropes

The condition of a SWR is desirable to know because it makes it possible to discard the rope at the right time, which is the favourable balance between safety and cost-efficiency, as extended service may jeopardise safety, and limited service increase cost. The condition of a SWR affects its capability to transfer tension force, either by weakening the material properties or reducing its cross-sectional area. Thus, common modes of deterioration and discard criteria are usually based on either weakening of the material properties or reduction in the cross-sectional area. According to [5, p.10-11], the common modes of deterioration of a SWR are

- Number of visible broken wires
- Decrease in rope diameter
- Fracture of strand(s)
- Corrosion
- Deformation
- Mechanical damage
- Heat damage

Further, [5, pp. 14-22] suggests five individual discard criteria, which are recommended to use only in the absence of any instructions provided by the supplier or manufacturer of either the rope or the crane it's used with. The criteria are based on

- Visible broken wires
- Decrease in rope diameter
- Fracture of strand(s)
- Corrosion
- Deformation and damage

In addition, a method for discarding a SWR based on the combined effects of the number of broken wires, decrease in diameter and extent of corrosion is presented in [5, pp. 42-44]. Most service discards are based on combined effects [7, p. 46]. Thus a combined criterion may be the most appropriate method of discarding a SWR. Many international standards and codes resort to subjective descriptions in methods of discarding based on combined deterioration [7, p. 46], and evaluation of corrosion in the method of [5, pp. 42-44] makes no exception.

As mentioned in Chapter 1, the most common discard criterion is the number of visible broken wires [2], [1, p. 260] claims that the most important discard criterion is the number of broken wires over a pre-defined length, for example, the SWR's lay length. [6, p. 72] observed that the number of wire breaks prior to rope failure is heavily dependent on the severity of the test conditions, as they observed many broken wires prior to failure in a rope tested under less severe conditions, and fewer under severe conditions, and none(!) under the most severe conditions. In [6] it is not explicitly written if the number of broken wires is visible or not, however, since no form of nondestructive testing (NDT) technique is mentioned, and the wire breaks are said to be counted as part of the procedure, it is assumed that the number of broken wires is actually the number of visible broken wires. Based on this research, discarding a SWR by the number of visible wire break's should be limited to specific ranges of operating conditions.

According to research by [8], [9], and [6, pp. 81-82], the SWR is known to be elongated in a characteristic pattern during fatigue bending tests. The elongation is initially large due to wire settling, followed by a longer period with more or less constant elongation, which is then again followed by a sharp increase in elongation before rope failure. According to [1, p. 260], for a variety of non-specified reasons, the increase in the rate of elongation of the rope often cannot be detected in practice. Even if it could be detected, [6, p. 81] reports that the characteristic pattern of elongation is dependent on the severity of the test conditions, with the sharp increase in elongation being non-present prior to rupture under more severe test conditions, implying that also discarding a wire based on elongation, should be limited to certain ranges of operating conditions.

2.2 Fatigue

Fatigue is the process where a material is exposed to cyclic loading, which leads to weakening of the material. For metals, this weakening typically takes the form of crack growth and may initialise in any material defect. Thus, it's nearly impossible to prevent it, as today's technology is unable to produce materials without microscopic imperfections. The initial crack grows a miniscule amount under each load cycle, and after a sufficient number of cycles results in material fracture. Thus, a material's fatigue life is commonly measured in the form of the number of cycles, from initiation to fracture, alternatively from initiation to some discard criteria. Fatigue is usually associated with tensile loads, however, [10] reports a case in which crack growth appeared under compressive loading.

2.2.1 Fatigue of steel wire ropes

The mechanisms of fatigue of SWR are not yet fully understood, and none of the currently existing fatigue models is directly applicable to calculate the remaining number of cycles based on its current condition. However, through a large number of experiments, the elements presented in the following are found to have an influence on the fatigue life of SWRs regarding the number of bending cycles [1, pp. 220-248], and not presented in any specific order.

Tensile force and diameter ratio

The tensile force S and the ratio between the sheave and rope diameter D/d, have the most important influence on the number of bending cycles [1, p. 220]. According to [1, p. 220], the breaking number of bending cycles drops abruptly when the specific tensile force becomes equal to, or greater than, the Donandt force. The breaking number of bending cycles is the amount of bending cycles tested before

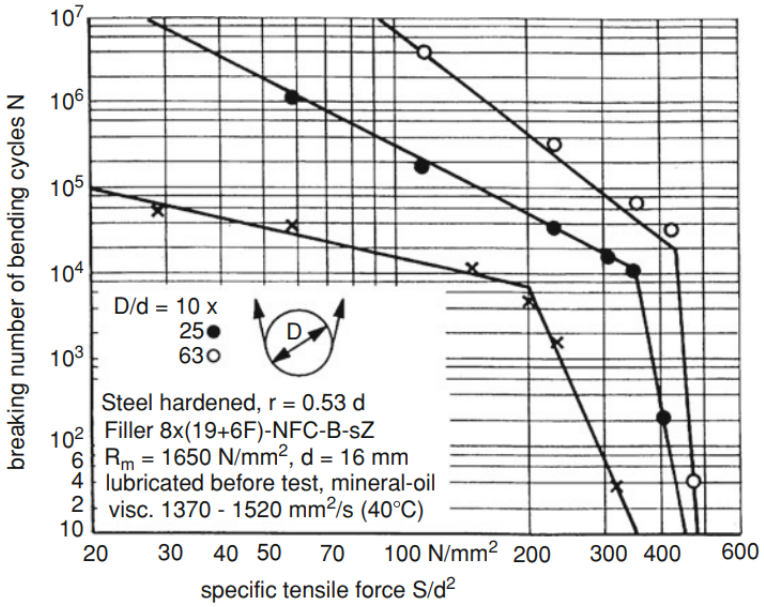

Figure 2.3: The breaking number of bending cycles as a function of specific tensile force, reproduced from [1, p. 220] with permission from copyright holder

the rope is so heavily damaged that the testing can not be continued, possibly because of a ruptured strand. The Donandt force is the magnitude of force at which the wires yield stress is reached. Thus, this is considered the maximum limit of the usable tensile force. The effects of the Donandt force on the breaking number of bending cycles is graphically displayed in Figure 2.3 together with the corresponding experiments it is based on. [11] and [12, pp. 115-119] established an equation which describes the number of bending cycles as a function of the rope strengths R_0, specific tensile force S/d^2 and of diameter ratio D/d, which is valid when the tensile force is less than the Donandt force

$$\lg N = a_0 + a_1 \cdot \lg\frac{S[mm^2]}{d^2[N]} + a_2 \cdot \lg\frac{D}{d} + a_3 \cdot \lg\frac{S[mm^2]}{d^2[N]} \cdot \frac{D}{d} \tag{2.2}$$

where a_0, a_1, a_2 and a_3 are, for now, undefined constants, D and d are in unit mm, and S is in unit N.

The ropes nominal strength

[8], [13], [15] and [16] have all carried out bending tests and observed a slight increase in fatigue life with increasing nominal rope strength, however, to a varying degree. With the basis in results obtained by [16], and others, [14] derived a regression calculation which defines the tensile force as a function of the ropes nominal strength R_0 to those with a nominal strength of 1700 N/mm^2

$$S = S_{1770}(\frac{R_0}{1700})^c \tag{2.3}$$

where S_{1770} is in unit N, R_0 is in unit N/mm^2 and c is, for now, an undefined constant.

With the basis in Equation (2.3), [1, p. 225] derived an equation for calculating the relative number of bending cycles between a rope with nominal strength R_0 and rope with nominal strength equal to 1700 N/mm^2, as

$$\lg\frac{N}{N_{1770}} = c \cdot (b_1 + b_3 lg\frac{D}{d}) \cdot \lg\frac{R_0}{1770} \tag{2.4}$$

where D and d are in the same unit, R_0 is in N/mm^2, and c, b_1 and b_3 are undefined constants.

The rope diameter, size effect

By keeping the influence of all the other parameters constant, [17] showed that the fatigue life is dependent on the SWR diameter, were increasing diameter reducing the fatigue life, when the rope diameter was larger, or equal to, $6mm$. These findings lead to the definition of an endurance factor for rope diameter f_d, which is a function of the SWR diameter. This endurance factor expresses the ratio between the breaking number of bending cycles of a SWR with diameter d, and bending length l equal to $60 \cdot d$, and a SWR with a diameter and bending length equal to 16 mm and $60 \cdot 16$ mm, respectively[1, p. 226]. This endurance factor can be calculated for a rope with diameter d by [1, pp. 227-228]

$$f_d = \frac{0.52}{-0.48 + (d/16)^{0.3}}, \ d \geq 6 \ mm \tag{2.5}$$

where d is unit mm.

Bending length, size effect

[18] carried out bending tests on SWRs with different bending lengths, and found that the number of bending cycles decreases as the bending length increases. These findings led to the definition of another endurance factor f_L, which takes into account the effects of the bending length. "The rope endurance is influenced only statistically by the rope bending length (statistical size effect). The number of bending cycles will vary across the rope bending length as a matter of probability", [1, p. 229]. Based on the work of [19] and [20] on probability, and the work of [17] on class- and solo standard deviation, [1, p. 231] derived an approximate equation to calculate the endurance factor influenced by the rope bending length l

$$f_L = \frac{1.54}{2.54 - (\frac{l/d - 2.5}{57.5})^{-0.14}}, \ l \geq 10 \cdot d \tag{2.6}$$

where l and d are given in the same unit.

Rope core and number of strands

[1, p. 289] presents an endurance factor f_C for rope core and number of strands, based on the work performed by [16], [21] and others, which showed that the fatigue life of a SWR is dependent on the type of core and number of strands. The numerical values of this factor for different types of cores and number of strands are presented in [1, p. 289].

Number of bending cycles

By taking the previously described elements into account, the number of simple bending cycles, i.e. the number of times a SWR is bent over half a sheaves circumference, can be calculated by [1, p. 287]

$$\lg N = b_0 + (b_1 + b_3 \cdot \lg\frac{D}{d}) \cdot (\lg\frac{S}{d^2} - 0.4 \cdot \lg\frac{R_0}{1770}) + b_2 \cdot \lg\frac{D}{d} + \lg f_d + \lg f_L + \lg f_C \tag{2.7}$$

where d is the nominal rope diameter in mm, D is the sheave diameter in mm, S is the rope tensile force in N, R_0 is the nominal tensile strength in N/mm^2 and l is the bending length. f_d and f_L are calculated by Equation (2.5) and (2.6), respectively. The constants b_0, b_1, b_3, b_2 and f_C can be found in [1, pp. 288-289].

The equation is valid under the following conditions [1, p. 288]

- The magnitude of the tensile force is less than the Donandt force
- $d \geq 6$ mm
- $l \geq 10 \cdot d$

- The wire rope is well-lubricated with viscous oil or Vaseline
- The sheaves have steel grooves with groove radius r, $r = 0.53 \cdot d$
- There is no side deflection
- The surrounding environment is considered dry

The number of bending cycles calculated by Equation (2.7) can be corrected by a set of endurance factors [1, pp. 289-290], which takes into account lubrication, side deflection, the pressure in the grooves, form grooves, and bending of twisted wire ropes. These factors are presented in the latter reference.

2.3 Condition monitoring techniques

CM is the process of monitoring a certain set of parameters, which for this thesis describes the condition of the SWR. The aim of CM is to identify and track developing faults, for maintenance to be scheduled at the appropriate time, or action to be taken to prevent consequential damage. The parameters regarding deterioration are presented in Section 2.1.1, while the parameters regarding fatigue are discussed in Section 2.2.1. Hence, we now turn our attention towards monitoring, more specifically the monitoring techniques. [3] reviewed the CM technologies applicable for SWRs, which is reported to be

- Electromagnetic method
- Acoustic emissions (AE)
- Ultrasonic Guided Waves
- Ionizing Radiation
- Fiber Optics
- Optical Computer Vision
- Thermovision
- Current Signature

Further, [3] states that the most common monitoring technique is the electromagnetic method, while a combination of techniques is the probable future for online condition monitoring of SWR. We now turn our attention towards the CM technologies that are used in this thesis, which are the electromagnetic method, AE and the optical computer vision. Additionally, the method of visual inspection is presented and briefly discussed.

2.3.1 Electromagnetic method

By magnetising a SWR along its axial axis, thereby making it the path for the magnetic circuit, magnetic dispersion forms as the magnetic flow exits one wire and enters a new one. This magnetic dispersion is detected in a leakage field test [22, p. 5], where the change in the radial leakage field component induces a voltage in the induction coil during the measurement. By amplifying and recording this voltage, the so-called basic signal in the measurement coil is obtained. The amplitude of this signal is a function of the rope's length, as shown in Figure 2.4. As the magnetic dispersion forms when the magnetic flow exits one wire and enters a new one, it follows that a breakage of a wire will form magnetic dispersion, and depending on the distance between the broken pieces of wire, the amplitude and nature of the base signal changes [22, p. 8]. Thus, in principle, it is possible to detect

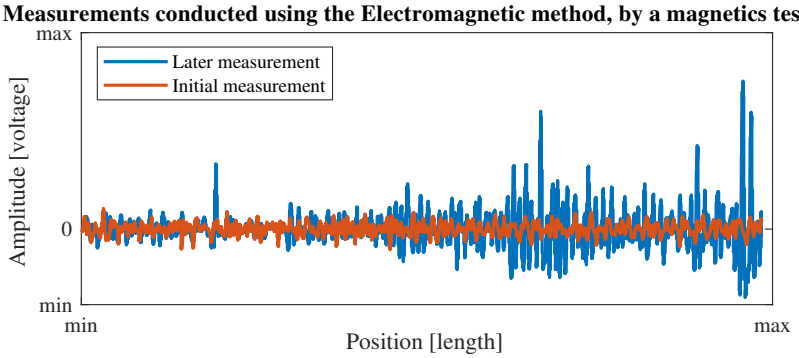

Figure 2.4: An example plot of the basic signal obtained by the use of a magnetics tester, which is a measuring instrument that uses the electromagnetic method, for an initial- and later measurement of a SWR

a wire breakage and track the potential increase in distance between the two pieces of the broken wire. If it is intended to use a magnetic tester on a rope during its lifetime, [5, p. 13] recommends an initial examination, preferably, after the rope has been installed, to serve as a reference point for future comparison. The initial examination enables comparison between the initial signal and signals obtained by measurements taken at a later time, as shown in Figure 2.4. This may make it easier to detect deterioration, as changes in the base signal's amplitude at a specific rope position imply a discontinuity in the magnetic flow field. According to ISO [5, p. 13], "non-destructive testing (NDT) by electromagnetic means may be used as an aid to visual inspection to determine the location of those sections of rope which could be suffering deterioration". According to [3, p. 6], manual and subjective interpretation of the measurements is one of the main challenges associated with the use of electromagnetic methods. Generally speaking, a magnetic tester detects local faults (LF) and loss of magnetic area (LMA). The magnetics tester used in this thesis is designed to detect wire breaks, which is a LF. However, it is believed that its measurements can be used to determine the LMA. [27] assumed that the loss of metallic area are linearly related to sensor voltage, and proposed the following equation to calculate the loss of metallic area

$$L_{ma} = U_h \frac{A_c}{U_{hc}} \tag{2.8}$$

where L_{ma} is the loss of metallic area, U_h is the magnetic tester's measured voltage of the SWR, A_c is the calibration rod area and U_{hc} is the mangetic tester's measured voltage of the calibration rod.

However, as by plugging in the numbers of the magnetic measurements obtained in this thesis, the loss of metallic area appear to be several times greater than the actual cross-sectional area of the tested SWRs. Hence, more research is needed on the latter equation, and the calculation of loss of metallic area and LMA aren't furthered considered in this thesis.

2.3.2 Acoustic emission

When a loaded material undergoes sudden internal changes, stress weaves are produced in the form of AE [3, p. 6]. Examples of internal changes are crack initiation and growth, two essential elements in fatigue of SWR. The stress weaves can be measured by a piezoelectric transducer, which produces an electric signal based on an analogue input. This electrical signal is further amplified, filtered, stored and analysed. An example of a hit based transient acoustic wave recording is presented on Figure 2.5 together with central terms of AE recording. The meaning of hit based is that the recording is only saved if the magnitude of the measurement is above a certain threshold, as displayed in Figure 2.5. The amount of energy released when a wire breaks is dependent on the load at the fracture [3,

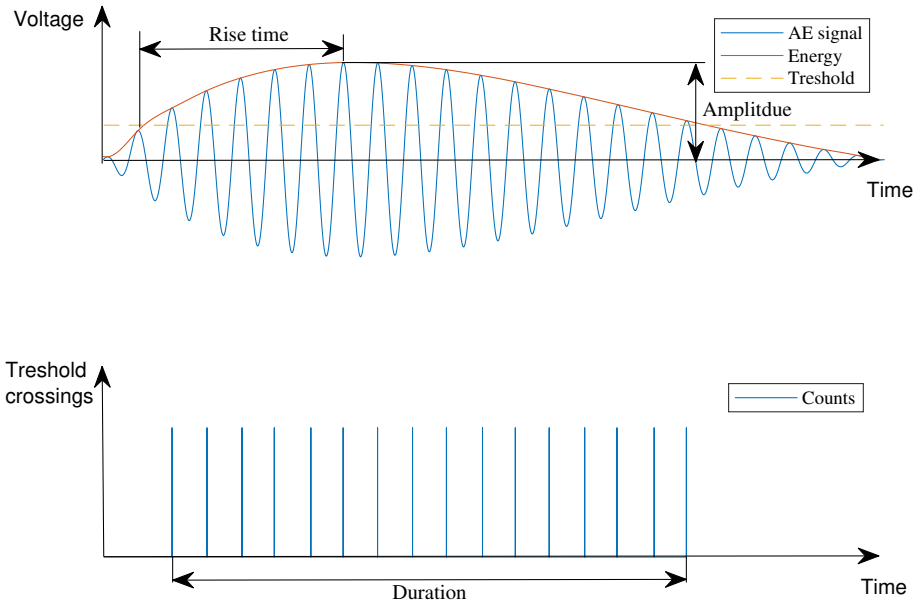

Figure 2.5: An example of a hit based transient acoustic wave recording together with central terms of AE recording. Only the parts of the AE signal which has a voltage higher than the threshold value is saved

p. 6]. Thus, if the wire breakage occurs with a low load at the fracture, typical for wires in bending applications, the fracture might not release enough energy to ensure successful and robust detection. Detection of acoustic emission in a wire is not limited to wire breaks, according to [23, p. 939] other important sources are interwire fretting and corrosion. However, [23] confirmed through a review of the method applied to wire monitoring that its most realistic application is detection and location of wire breaks and that the associated challenges are

- The signal is quite effectively dampened in the air. Thus the recorder has to be located close to the source
- It is difficult to determine between which strand the wire breaking occurred
- Successful detection is dependent upon the rope construction, diameter, length and number of wire breaks
- The rope needs continuous monitoring as the wire breaking effect is irreversible due to the Kaiser effect

Before the analog AE measurements can be saved to a computer, they must be converted from analog to digital form. This happens in rate known as the sampling rate, which is determined by considering the frequency of the elements that is to be measured. In theory, by the Nyquist–Shannon theorem, the sampling rate should be at least twice the highest data frequency of the sampled signal, in practise however, a frequency that is 5-10 times higher must be chosen[25, p. 10].

Theory of custom AE sensor system

In this thesis, a custom AE sensor system is utilised. The theory behind this system is presented in this section, while the actual custom AE sensor system is presented in Section 3.3.2. The reader may find it useful to study the latter section before trying to understand the theory behind the system.

The custom AE sensor system is regarded as innovative due to the analog pre-processing it performs on the recorded AE. The motivation behind this pre-processing is to enable the use of low cost and low sampling rate digital acquisition (DAQ) equipment, which produces relatively small amounts of data to be processed and stored, thus, reducing system cost. The technique is based on heterodyning the amplified the AE signal with a carrier signal. Hetrodyning is the process of multiplying the original signal with another signal, in thesis a carrier signal, to change the frequency of the original signal. The frequency of the carrier signal can be chosen freely, thus, enabling the system to be adapted for any AE phenomenon of interest within the sensitivity frequency range of the AE sensor, which according to [26, p. 3], typically is the limiting component of an AE sensor system. Next, the signal envelope is obtained by phase shifting the heterodyned signal by $\pi/2$. Thus, creating an analytic signal that is digitally sampled. This reduces the need for a small sampling time.

2.3.3 Optical computer vision

A digital image is composed of pixels having a color value. If we assume that the image has a red green blue (RGB) color model, the color is the sum of the red-, green, and blue light, where each light has numerical value between 0 and 255, thus, enabling 256^3 different colours.

As visual inspection is the main method of inspecting a SWR, optical computer vision is believed to have the potential of becoming a prominent inspection method. However, as experienced in the tests in this thesis, there are several significant challenges associated with optical computer vision for SWR inspection, which according to [3, p. 9] are

- Surface contamination by e.g. oil, mud, organic growth and even water
- The method is not applicable for internal wire breakings
- Outdoor lighting conditions are challenging, but can be removed by boxing in the camera and use active light source
- Obtaining sufficient number of supervised training data sets for all fault classes

The field has seen a considerable development over the last couple of decades [3, p. 9]. Using optical computer vision, [28] managed to obtain a precise estimation of the lay length of a strand, by utilising information about the structure and appearance of a SWR. This technology is now commercially available through Winspect GmbH.

2.3.4 Visual inspection

In the absence of any instructions provided by either the manufacturer or supplier of the rope itself or the crane it is used with, [5, p. 10] recommends daily visual inspection of the working section of the SWR. The purpose of visual inspection is to detect abnormalities in the SWR, such as broken wires or corrosion, and to possibly track their development.

Chapter 3

Apparatus

3.1 Continuous bend over sheave rope testing machine

In order to emulate the industrial application of the SWR, at least in terms of offshore hoisting applications, it is tested by a method that the International Organization for the Study of Ropes (OIPEEC) [29] defines as *simple bending*, which is that a wire is applied tension and continuously bent over a single sheave. This test method is also known as cyclic bend over sheave (CBOS) and it's illustrated in Figure 3.1 together with the basic terminology of the test set-up. The CBOS rope testing machine used in this thesis is presented in Figures 3.2-3.3, it's produced by DEP Engineering in conjunction with Teknova, University of Agder (UIA) and Mechatronics Innovation Lab (MIL), and located at MIL, Grimstad, Norway. It has the capacity of 15 kN line-pull, and can be used with wires which have a diameter in the range of 20-30 mm. The traction sheave has a diameter of 1000 mm, while the test sheave has a diameter of 800 mm. The machine has a trolley which the SWR is mounted to, and it counts a cycle when the trolley has returned to its start position. A picture of the trolley in its start position is presented in Figure 3.4. The machine is designed to move the rope throughout the range of this trolley, and, as a result, some parts of the SWR is bent over the entire circumference of the sheave, each counted cycle. Thus, by the definition of simple bending test of [1, p. 214], every counted cycle corresponds to two simple bending cycles. Hence, in this thesis, the reported number of cycles which a SWR endured is the number of simple bending cycles, not the counted number of bending cycles by the machine. The section of the SWR which is bent over the entire circumference of the test sheave is called the double-bending zone. Other parts of the SWR which are bent once every cycle, is referred to as the single-bending zone, and the parts that are not bent at all are referred to as the non-bending zone.

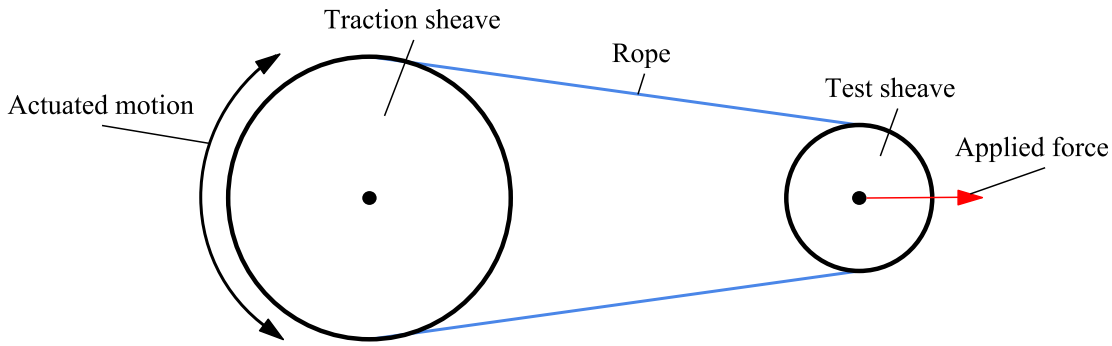

Figure 3.1: Illustration of simple bending test method together with basic terminology of the test set-up

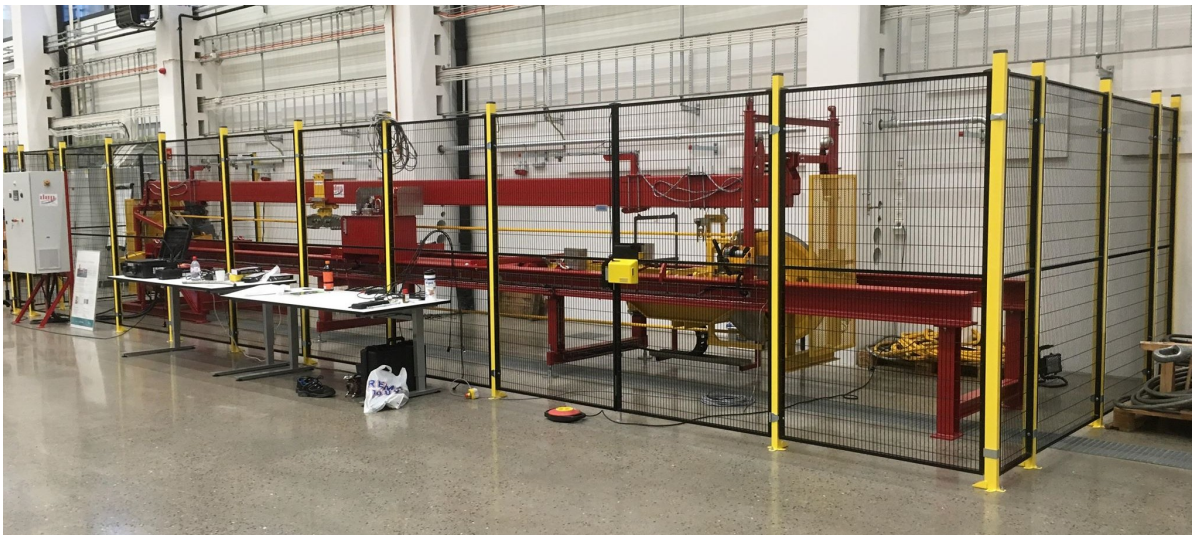

Figure 3.2: An overview of the CBOS rope testing machine used in this thesis

Figure 3.3: The CBOS rope testing machine shown from the backside. The test sheave is visible on the left side. As shown, a yellow fibre rope is mounted at the time this picture was taken

Figure 3.4: The trolley of the CBOS machine shown in its start position with a SWR mounted to it. The machine counts a cycle every time the trolley returns to this position

3.2 Magnetic tester

The magnetic tester used in this thesis is presented in Figure 3.5. It was developed by the University of Stuttgart, Institute of Mechanical Handling and Logistics, and is named Stuttgart Magnetic Rope Tester (SMRT) 40. It can be used to test ropes with diameter from 16 mm up to 40 mm for full locked coil ropes, or up to 45 mm for stranded wire ropes, and is designed to detect wire breaks. Additionally, the maximum metallic cross-section is 1000 mm^2. It measures distance with the surveyor's wheel, which is visible on the left of Figure 3.5a. The magnetic tester is equipped with coils of dimensions that are determined by the SWR its used with. In this thesis, the 35 and 40 mm coils are utilised for the 24 and 26 mm SWRs, respectively. Ideally, the 35 mm coil should have been used for both rope diameters as its recommended to use with ropes of diameter $23 - 26$ mm, however, the 35 mm coil was damaged after it had been used with the 24 mm rope, hence, the 40 mm coil was used with the 26 mm ropes, although its recommended to use with ropes of diameter $27 - 31$ mm.

(a) The SMRT 40 free standing with mounting bracket

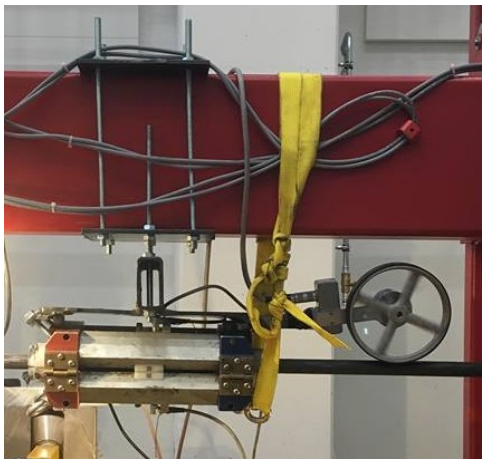

(b) The SMRT 40 mounted

Figure 3.5: The magnetic tester used in this thesis (SMRT 40), free standing with mounting bracket in (a) and mounted in (b)

3.3 Acoustic emission sensor system

Two different AE sensor systems are used in this thesis. MISTRAS produces one of them, and the other is custom made, hence, they are later referred to as the MISTRAS- and custom AE sensor system.

3.3.1 MISTRAS AE sensor system

The MISTRAS AE sensor system consists of an AE sensor, signal amplifier and Peripheral Component Interconnect (PCI) coupled to a ordinary computer, which has the corresponding software from MISTRAS installed. The signal amplifier, sensor, and corresponding cables are identical to those of the custom AE sensor system, and are presented in Section 3.3.2. The gain of the signal amplifier is set to $40dB$. The system is hit based, which means that recorded signals are only saved if their amplitude exceeds a pre-defined threshold value. In this thesis, this threshold value is set to 60 dB. The purpose of this threshold is to reduce the amount of data recorded, as recordings below this threshold is believed to be of little interest.

The system measures the

- Type of event, either AE hit or time based

- Time and date of event
- Parametric - the raw voltage delivered to the Parametric Input socket on the PCI
- Cycle - counts the number of cycles based on the Parametric reading and preset range, e.g. load cells or pressure sensors can be used for generating cycles.
- Channel - sensor channel on input board
- Risetime - time from first threshold crossing to highest voltage point on the waveform in unit μs. The risetime is graphically displayed in Figure 2.5
- Counts - the number of times the signal crosses the detection threshold. Counts are graphically displayed in Figure 2.5
- Energy - time integral of the absolute (ABS) signal voltage. The reported magnitude depends on the value selected for Energy Reference Gain. Proportional to signal strength.
- Duration - time from first to last threshold crossing in unit μs. The duration is graphically displayed in Figure 2.5
- Amplitude - highest voltage in the AE waveform, expressed in dB_{AE} amplitude scale. The amplitude is graphically displayed in Figure 2.5
- Average frequency - counts divided by duration, divided by 1000 (i.e. kHz). Note that this is not a spectral domain calculation, but a calculation from time domain features
- Root mean square (RMS) - RMS voltage during a period of time based on a time constant of 500 ms, referred to the input to the signal processing board.
- Average signal level (ASL) - RMS converted to dB_{AE} scale ($0dB_{AE} = 1\mu V$) at the sensor before any amplification. A more formal definition is given by [30]: "n-the rectified, time averaged AE logarithmic signal, measured on the AE amplitude logarithmic scale and reported in dB_{AE} units, (where $0dB_{AE}$ refers to 1 pV at the preamplifier input)".
- Threshold - detection threshold, on the dB_{AE} scale. The treshold is graphically displayed in Figure 2.5
- Reverberation frequency - (counts - counts to peak) divided by (duration - risetime)
- Initiation frequency - counts to peak divided by risetime
- ABS energy - time integral of the square of the signal voltage at the sensor before any amplification, divided by a 10 $k\Omega$ impedance and expressed in unit aJ (attojoules)
- Frequency Centroid - the centre of mass of the power spectrum
- Peak Frequency - the point where the power spectrum is greatest
- Counts to peak - number of threshold crossings from first to highest voltage point on the waveform
- Signal strength - time integral of the ABS voltage, expressed in pVs (picovolt seconds) referenced to the sensor, before any amplification. Proportional to Energy.

Further, the sampling rate is set to 2 MHz, hit defination time (HDT) to 120 μs, hit lockout time (HLT) to 120 μs and peak definition time (PDT) to 60 μs. HDT, HLT and PDT are timing parameters of the signal measurement process. "In brief, a proper setting of PDT ensures correct identification of the signal peak for risetime and peak amplitude measurements. Proper setting of the HDT ensures that each AE signal from the structure is reported as one and only one hit. With proper setting of the HLT, spurious measurements during the signal decay are avoided and data quisition speed can be increased." [31, p. 17].

3.3.2 Custom AE sensor system

The custom AE sensor system is presented in Figure 3.6 together with the name referencing to its main components, which are, and have the corresponding function

- Preamplifier, amplify the electric charge from the piezoelectric transducer sensor, i.e. the AE sensor
- AE sensor, detect and convert acoustic energy into electric charge
- Signal generator, generate the carrier signal
- Analogue processing board, process the carrier signal and the signal from the preamplifier, i.e. create the envelope by utilising the Hilbert transformation
- DAQ, converts the analogue signal into a digital signal, enabling computer processing of the measurements

A description of the components in the AE sensor system is presented in Table 3.1. As seen in this table, two DAQs are listed, and unless otherwise specified, the DAQ from National Instruments are used in the custom AE sensor system. The system is designed in such a way that the polarity of two input voltage channels can change during a measurement. In this thesis, the recording duration of each AE performed with this system is set to 10 minutes, with a sampling rate of $10,000$ SPS (samples per second). With the current system, this sampling rate proved to be sufficient to monitor crack growth in an aluminium test piece during tension-tension fatigue test [26]. By human error, the frequency of the signal generator is set to 111 kHz. As the MISTRAS AE sensor system was scheduled to be used in the first test, and the custom AE sensor systems in the second, third and fourth, the intention was to use the AE measurements from the MISTRAS system to identify the appropriate measurement frequency of the custom AE system. The appropriate measurement frequency was to be identified by plotting the ABS energy as a function of Centroid frequency, as shown in Figure 3.7, to identify what the frequency of the measurements with highest ABS energy was, as those are the ones which are believed to be wire breaks. Based on the plot in the latter figure, it seems that a frequency closer to 400 kHz would have been more appropriate than the selected frequency of 111 kHz. The gain of the signal generator is set to 20 dB, which is the lowest possible setting. Unlike the MISTRAS-, the custom AE sensor system saves all recorded data. As we will see in the results, the custom AE system measures voltage in two channels, the reader might be confused about how this can be when the system only utilises one sensor. As mentioned in Section 2.3.2, the system phase shifts the heterodyned signal by $\pi/2$. Hence, the measured voltage in the second channel is the voltage in the first channel with a $\pi/2$ phase shift.

Component	Model & Description
AE Sensor	MISTRAS R15a, pn# R15a, SENSOR, 150KHZ W/SubMiniature version A (SMA) CONNALPHA S
AE Sensor cable	MISTRAS 1232-SMA/BNC-2, pn# 1232-4001-002, SENSOR CABLE, Bayonet Neill–Concelman (BC) TO SMA, 2M (For Alpha sensors)
Preamplifier	MISTRAS 2/4/6 Type C Preamplifier, pn# 1220-5045, 2/4/6 singlended/differential AST preamplifier with a 2/4/6 series filter (Filter Range: 100HP), powered by 28V DC through a separate BNC
Signal cable	MISTRAS 1234-BNC/BNC-10 m, pn# 1234-2, SIGNAL CABLE, RG-58, BNC - BNC, 2M1
Signal generator	BK Precision 10 MHz Sine/Square Wave Generator Model 3003
Analog processing board	Processing board (PCB) with analog heterodyne, filtering and Hilbert transform with real and imaginary parts as two separate outputs
DAQ	National Instruments USB-6211 Measurement Computing USB-1608G

Table 3.1: Description of the components in the AE sensor system

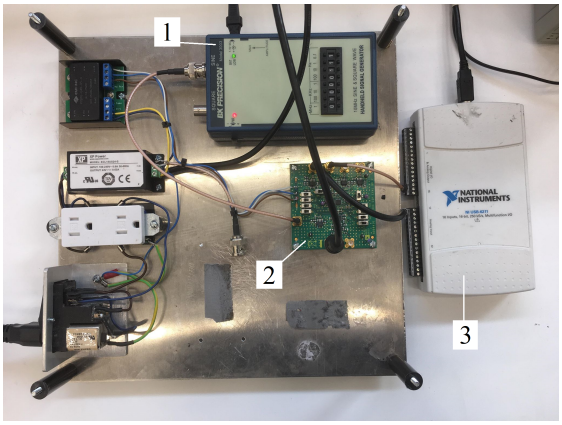

Figure 3.6: The custom AE sensor system used in this thesis. With reference to this figure, 1 is the signal generator, 2 is the analog processing board, and 3 is the data acquisition from National Instruments

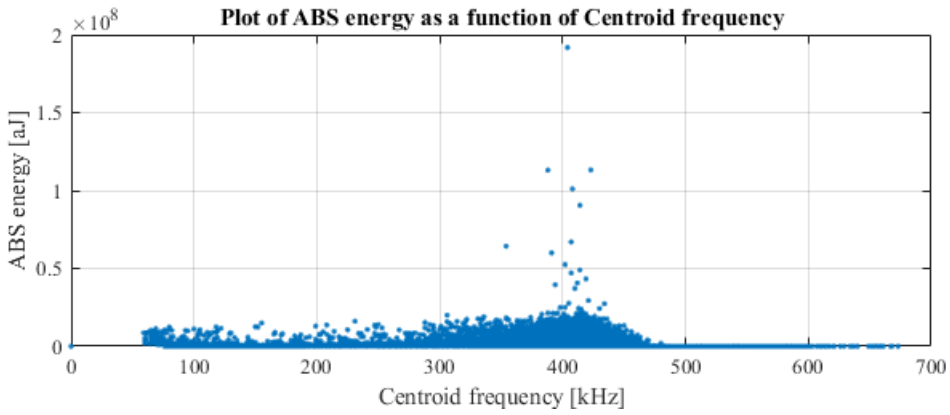

Figure 3.7: The ABS energy as a function of Centroid frequency, obtained from the measurement of the MISTRAS AE sensor system in the first test

3.4 Camera system

The camera system used in this thesis is shown mounted to the frame its used with in Figure 3.8 and consists of three cameras which point towards the SWR at an approximate angle of 120^o to each other. Thus, covering the whole circumference of the SWR. Specifications of the cameras are presented in Table 3.2. One of the cameras are delivered by BASLER, and the two other by Edmund Optics. For later reference, we will refer to the BASLER camera as camera 1, and the Edmund Optics cameras as camera 2 and 3. To improve the conditions of the cameras, additional special camera lights are installed together with a light-diffuser. The lights are light-emitting diodes (LED), have a 17W power draw with output comparable to a 150W Tungsten, and are delivered by Lightpanels. Three of these lights were utilised in this thesis and a picture of one of them is presented in Figure 3.9.

Figure 3.8: The camera system shown mounted to the frame its used with

Figure 3.9: One of the three LED lights used to improve camera conditions in this thesis, shown with a tripod mount

Producer	Model number	Resolution	Maxiumum FPS
Edmund Optics	EO-13122C	1280 x 1024	169
BASLER	acA1300-200uc - Basler ace	1280 x 1024	203

Table 3.2: Specifications of the cameras used in this thesis

Chapter 4

Methodology

As mentioned earlier, the objective of this thesis is to identify measurable and quantifiable features of the SWR which indicate deterioration, by utilising the data obtained by the use of a magnetic tester, an acoustic emission sensor- and a camera system. The magnetic tester is used to identify and track discontinuities in the cross-sectional area of the rope, possibly due to broken wires or stands. The AE sensors system(s) are used to identify and track the development of broken wires. Additionally, visual inspection is used to count the number of broken wires, however, only in the first test. Thus, to summarise, we are using the magnetic tester, AE sensor system and visual inspection to cover broken wires, while the camera system is used to track the potential change in diameter and lay length.

As part of the post processing of the data-sets of AE- and magnetic measurements, several statistical tools are applied to determine how the measurements can be utilised to identify deterioration. The statistical tools applied in this thesis on the AE- and magnetic measurements are the largest magnitude-, RMS- and the integral of magnitude as a function of cycle or event. In all tests, the recordings of the camera system are taken when the SWR carries the tensile force specified in the corresponding test specification. Measurements using the magnetics tester are conducted manually. The camera system is automated to film the rope for 20 seconds every 1000 cycles, thus, filming the part of the SWR which passes by the cameras during a cycle at least one time, while the AE sensor system(s) measures continuously throughout the test. As using the AE sensor system to detect broken wires in SWR is a relatively new concept, the literature has not yet agreed which location that is most suited for AE sensor mounting, therefore, three different positions for the AE sensor are tested. All the SWRs tested in this thesis are discarded based on the same discard criterion, which is that the machine is programmed to stop when the rope has a sharp decrease in its ability to transfer tension force.

4.1 First test

The aim for this test was to identify which of the measured quantities of the Mistras AE sensor- and the camera system that indicate deterioration of the SWR, and test the positioning of the AE sensor which is directly mounted to the rope, as shown in Figure 4.1, by the use of a steel u-bolt and epoxy. Ideally, the u-bolt should consist of a material which is more suited to transfer AE signals, such as aluminium. However, aluminium u-bolts were not available at the time the test took place. The function of the epoxy is to glue the sensor to the u-bolt, and at the same time serve as a more efficient transmitter of AE signals than air. Such a mounting is believed to have a good transfer of the AE generated by the rope. However, it might not be appropriate for industrial usage, as the sensor and corresponding mounting are unfit to travel over a drum or a sheave, thus limiting the operational use of the SWR its mounted to. The AE sensor system is expected to record an enormous amount of data. However, a lot of this data is believed to be noise. Hence the data is filtered, and all recordings with energy less than 200 J are excluded from post-processing and documentation. Further, the measured variables

which have a characteristic pattern through the fatigue life of the SWR, i.e. an exponential increase before the end of the ropes fatigue life, are identified, simply by plotting them. Those who have, based on qualitative judgement, are further investigated for correlation, not only for the data set as a whole but also for correlation trends, i.e. changes in correlation during the SWR fatigue life. Lay length and diameter measurements using the camera system are performed on the same location on the SWR, on the recordings done at cycle 500, i.e. the first recordings after the initial settling of the SWR is believed to be complete, and 39500, i.e. the last video recorded by the camera system before the SWR was discarded. Finally, a manual inspection of the rope after it is discarded is carried out to count the number of broken wires, and possibly strands, with the purpose of relating it to the measurement data obtained by the AE sensor system, and to gain more insight in the amount of damage a rope tested with our discard criterion has experienced. For example, if we had five ruptured strands, and five AE hits with very high energy, we could draw a connection between the two findings. After the SWR is discarded, it is separated into individual strands. Further, the number of broken wires in each strand are counted. The strands are expected to be covered in grease. Hence, each strand is flexed by hand during the counting process, with the purpose of making it easier to detect a broken wire.

The test specifications are presented in Table 4.1, and are the minimum specifications for defining a wire rope-bending fatigue test according to the International Organization for the Study of Ropes (OIPEEC), Recommendation No. 4, OIPEEC Bulletin No. 56 (1988). An attempt is given to follow these recommendations as closely as possible in all fatigue tests included in this thesis.

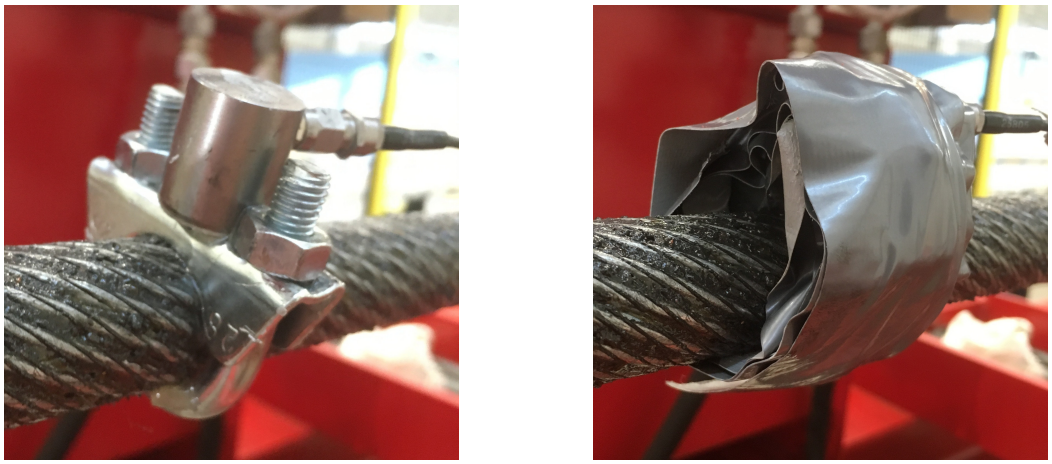

(a) The sensor mounting shown without tape

(b) The sensor mounting shown with tape

Figure 4.1: The AE sensor directly mounted to the SWR by the use of a u-bolt, tape, and epoxy. The u-bolt serves as a stable interface, the epoxy as AE signal transmitter, and the tape as increased assurance to prohibit the sensor from falling to the ground if the epoxy for some reason is to fail.

Test specifications	– Kind of bending: Simple bending – Tensile force, $S = 14700\ N$ – Bending length, $l = 4.2\ m$ – Rope temperature (if more than 50 ^{o}), $T_R < 50^oC$ as measured by heat radiation measurements displayed in Figure 4.2 – Deflecting angle (if less than 30 ^{o}), $\varphi_D > 30\ ^o$ – Lateral deflection angle, $\theta = 0\ ^o$
Wire rope specifications	– Wire rope construction, Dyform 34 x7 LR (16/6&6/6/1) – Wire lay direction, Right hand langs lay (zZ) – Nominal rope diameter, $d = 26\ mm$ – Measured rope diameter, $d_m = 26.82\ mm$ – Nominal wire strength, $R_0 = 1960\ N/mm^2$ – Mean measured wire strength, R_m, not measured – Minimum breaking force, $F_{min} = 623\ kN$ – Measured breaking force, F_m, not measured – Kind of lubrication, BRILUBE 20, a wax based lubricant specifically developed for wire ropes. Contains mineral hydrocarbon wax, synthetic wax, polymers and additives. – Viscosity of lubricant, dynamic viscosity $\mu = 0.08\ Pa \cdot s$ (tested at a plate at 130^oC) – Lubricated before and/or during test, lubricated before test by manufacturer
Sheave specifications	– Sheave diameter (groove ground), $D_0 = 768.5\ mm$ – Sheave material, tempered steel: 42CrMo4 T – Sheave hardness, 235-295 HB (Hardness Brinell) – Groove form, Rounded V-groove form with $\gamma = 40^o$, as illustrated in Figure 4.3 – Groove radius, $r = 16.35 \pm 0.15\ mm$, also illustrated in Figure 4.3

Table 4.1: Test specifications of the first test. The data sheet of the SWR is included in Appendix A

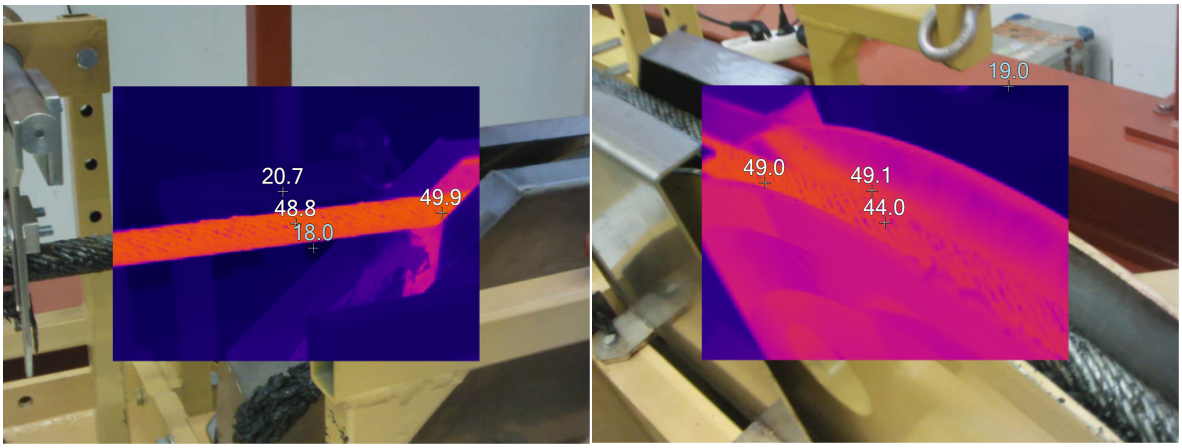

(a) Measurements at the exit of the test sheave, which is defined in Figure 3.1

(b) Measurements on the top side of the test sheave

Figure 4.2: Heat radiation measurements of the SWR, conducted after the machine had been running for 24 hours. Thus, the thermal steady state is believed to be achieved. The numerical values shown in Figures 4.2a and 4.2b are in unit ^oC, with emissivity set equal to 1

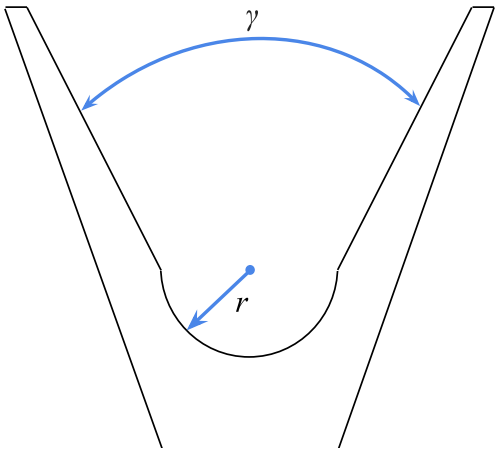

Figure 4.3: Illustration of the groove of the test sheave with groove radius r and groove angle γ

4.2 Second test

The aim of this test is to detect wire breaks using the custom AE sensor system, test whether or not a static interface serves a suitable location for the AE sensor, identify and track developments of discontinuities in the cross-sectional area of the rope using the magnetic tester, and once again test if the camera system can detect changes in lay length. As diameter measurements were unsuccessful in first test, new diameter measurements are not conducted in this- and further tests. The static interface is shown in Figure 4.4 and consists of a machined aluminium block, which is through water is in contact with the SWR. Both aluminium and water are great transmitters of AE signals, and this form of mounting is believed to have high industrial value, as it does not limit the use of the SWR it is mounted to. This specific interface had a high leakage of water. Thus, it relies on continuous water

supply, which has a temperature of approximately 9.2 ^oC. Hence, are believed to have a significant cooling effect, which is confirmed by considering the heat radiation measurements presented in Figure 4.6. The tests were otherwise performed in ambient test conditions. Similar to the MISTRAS AE sensor system, the custom AE sensor system is expected to record a massive amount of data. Hence, to make the post-processing less computational demanding all recordings are filtered, by excluding events which a voltage within the mean ± 4 standard deviations of the specific recording, from the post-processing and documentation. An example of the effect of such filtering is presented in Figure 4.5. The magnetic tester is mounted to the CBOS machine and SWR throughout the test, as shown in Figure 3.5b, with measurements conducted every 1,000 cycles. Similar to the first test, lay length and diameter measurements using the camera system are performed on the same location on SWR, on the first recordings done after the initial settling of the SWR is believed to be complete, and on the last recording by the camera system before the SWR was discarded. The specifications of this fatigue test are presented in Table 4.2.

(a) The static interface mounted to the CBOS machine (b) The static interface dismantled

Figure 4.4: The static AE sensor interface, by reference to these figures, 1 is AE sensor, 2 is the machined aluminium block, 3 is water nozzle, and 4 is machined plastic blocks. A continuous water supply is connected to the nozzle, i.e. 3 in the figures.

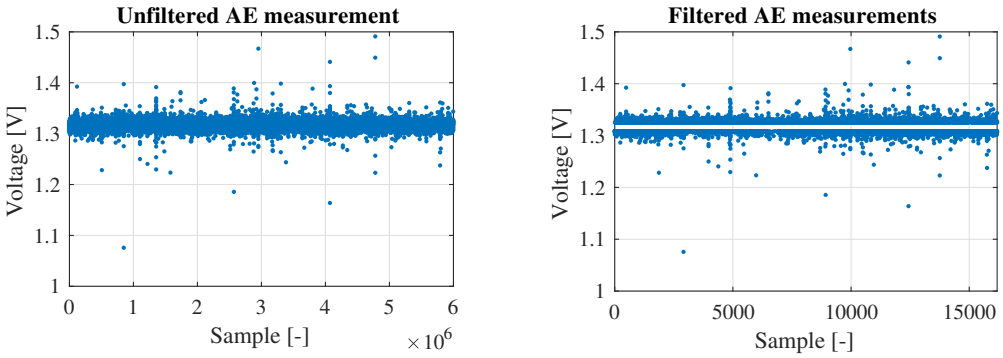

(a) Unfiltered AE measurement (b) The same AE measurement filtered

Figure 4.5: An example of how an AE measurements is affected by the chosen method of filtering

Test specifications	– Kind of bending: Simple bending – Tensile force, $S = 10700\ N(unit)$ when $N(cycle) \leq 45500$, $S = 14500\ N(unit)$ when $N(cycle) > 45500$ – Bending length, $l = 5.4\ m$ – Rope temperature (if more than 50 ^{o}), $T_R < 50^oC$ as measured by heat radiation measurements displayed in Figure 4.6 – Deflecting angle (if less than 30 ^{o}), $\varphi_D > 30\ ^o$ – Lateral deflection angle, $\theta = 0\ ^o$
Wire rope specifications	– Wire rope construction, Dyform 34 x7 LR (16/6&6/6/1) – Wire lay direction, Right hand langs lay (zZ) – Nominal rope diameter, $d = 24\ mm$ – Measured rope diameter, $d_m = 24.30\ mm$ – Nominal wire strength, $R_0 = 1960\ N/mm^2$ – Mean measured wire strength, R_m, not measured – Minimum breaking force, $F_{min} = 531\ kN$ – Measured breaking force, F_m, not measured – Kind of lubrication, BRILUBE 20, a wax based lubricant specifically developed for wire ropes. Contains mineral hydrocarbon wax, synthetic wax, polymers and additives. – Viscosity of lubricant, dynamic viscosity $\mu = 0.08Pa \cdot s$ (tested at a plate at 130^oC) – Lubricated before and/or during test, lubricated before test by manufacturer
Sheave specifications are identical to those presented in Table 4.1	

Table 4.2: Test specifications of the second test. The data sheet of the SWR is included in Appendix B

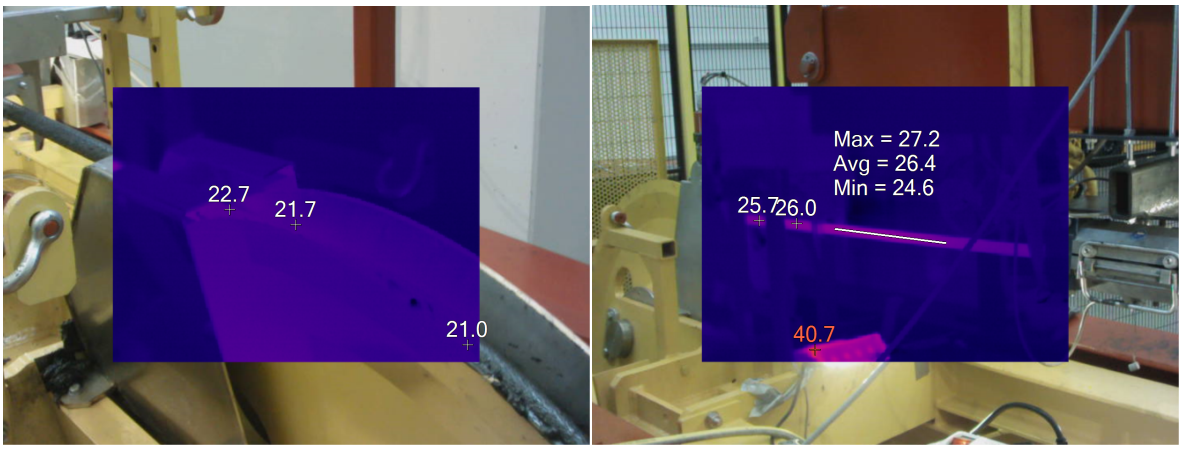

(a) Measurements on the top side of the test sheave, which is defined in Figure 3.1

(b) Measurements at the exit of the test sheave

Figure 4.6: Heat radiation measurements of the SWR, once again, conducted after the machine had been running for 24 hours. Thus, the thermal steady state is believed to be achieved. The numerical values shown in Figures 4.6a and 4.6b are in unit ^oC, with emissivity set equal to 1. Max, Avg and Min denotes the maximum, average and minimum temperature, respectively, along the white line shown in Figure 4.6b

4.3 Third test

This test aims to gather more data from the magnetic tester, custom AE sensor- and camera system. The AE sensor is directly mounted to the rope, similar to the first test, as shown in Figure 4.1. The AE measurements are filtered in the exact same manner as the AE measurements of the second test. This method is presented in Section 4.2 with an example shown in Figure 4.5. Once again, the magnetic tester is attached to the CBOS machine and SWR throughout the test, as shown in Figure 3.5b, with measurements conducted at a non-fixed interval. The cameras are re-positioned to make the best out of the limited number of light sources available. Thus, they are set to film the rope from the same angle, as shown in Figure 4.7. Measurements of the lay length are carried out in the same manner as for the first. As mentioned in Section 4.2, since diameter measurements were unsuccessful in first test, new diameter measurements aren't conducted in further tests. The test specifications for this test is identical to those of the first test, which are presented in Table 4.1.

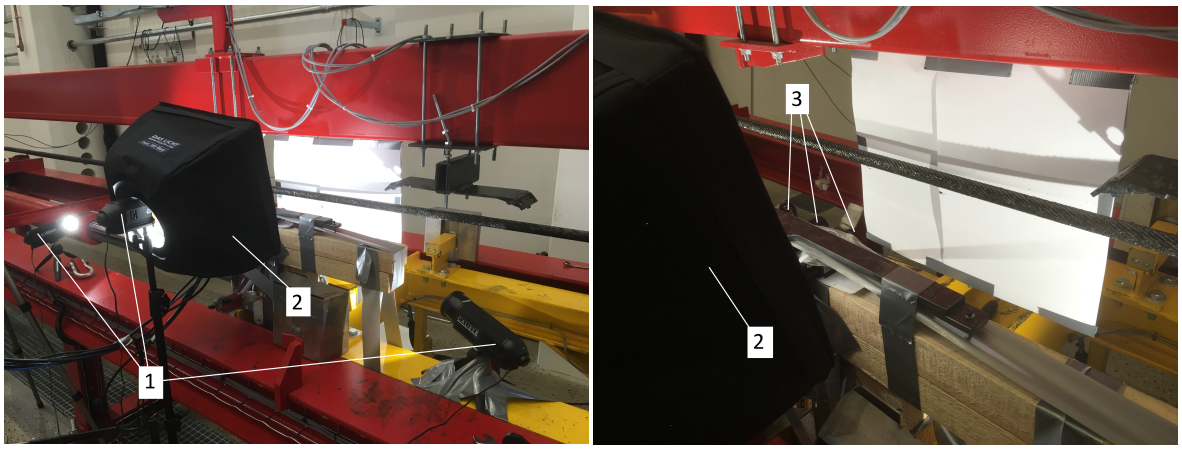

(a) Overview of the camera setup

(b) Overview of the camera setup with increased zoom, compared to Figure 4.7a, around the actual cameras from a slightly different orientation

Figure 4.7: The cameras shown in the new position. The three cameras are taped to a wooden beam which positions them at the right height, i.e. the same height as the SWR. With reference to these figures, 1 are the light sources, 2 is the diffuser, and 3 are the cameras

4.4 Fourth test

The aim of this test is similar to the third test, i.e. gather more data from the magnetic tester, custom AE sensor- and camera system. The AE sensor is directly mounted to the sheave, as shown in Figure 4.8. Based on the test results of the custom AE sensor system in the third test, one or more technical errors are believed to be present in the system, possibly in the DAQ. Hence, in the fourth test, the DAQ in the custom AE sensor system is switched from National Instruments USB-6211 to Measurements Computing USB-1608G, both presented in Table 3.1. Once again, the AE measurements are filtered by the same method as the AE measurements of the second test. This method is presented in Section 4.2 with an example in Figure 4.5. Similar to the third test, the magnetic tester is attached to the CBOS machine and SWR throughout the test, as shown in Figure 3.5b, with measurements conducted at a non-fixed interval, and the cameras are re-positioned to make the best out a limited number of available light sources, as shown in Figure 4.7. Measurements of lay length are also carried out in the same manner as for the first and second test. Once again, as mentioned in Section 4.2, since diameter

measurements were unsuccessful in the first test, new diameter measurements aren't conducted in further tests. The test specifications for this test is also identical to those of the first test, which are presented in Table 4.1.

(a) The paint of the sheave is removed as it's believed to dampen AE signals

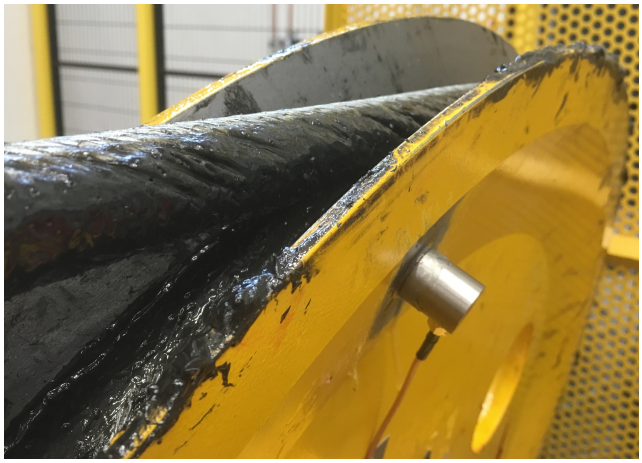

(b) The sensor is mounted at the location which is believed to have the shortest distance to the SWR since the material of the sheave is steel which is known to have a dampening effect on AE signal

Figure 4.8: The AE sensor directly mounted to the sheave by the use of epoxy

Chapter 5

Results and Discussion

5.1 First test

The rope endured 79,866 cycles before the discard criterion was met. A picture of the rope after it had been discarded is presented in Figure 5.1. The measured AE variables which had a characteristic pattern through the life of the SWR was the ABS energy, amplitude, ASL, energy, and RMS, as shown in Figure 5.2. Further, correlation trends were discovered between the ASL and ABS energy, energy and ABS energy, energy and ASL, energy and RMS, and, RMS and ABS energy, as shown in Figure 5.3. Each point of the correlation trends plots constitutes the correlation coefficient of the 1000 sequential events. Hence the number of data points of the correlation trends in Figure 5.3 is equal to that of Figure 5.2 divided by a 1,000. Additionally, the accumulated absolute energy for events with absolute energy more than $1 \cdot 10^6$ aJ are presented in Figure 5.4, which shows the characteristic pattern of a three-phase fatigue process, consisting of

- Phase 1, initiation, with minimal activity.
- Phase 2, slow and steady increase of accumulated ABS energy.
- Phase 3, sharp increase in accumulated ABS energy prior to SWR being discarded.

Measurements of diameter and lay length based on the videos filmed by the camera system are presented graphically in Figure 5.5 and 5.6, and numerically in Table 5.1 and 5.2, respectively. The diameter is expected to decrease and when considering the change in diameter presented in the last table, the change in rope diameter appear to be smaller than measurement error, as the diameter is unlikely to increase and decrease at approximately the same location. By Table 5.2, the lay length seem to have a slight decrease. As none of the cameras can capture the entire lay length of the SWR in one frame, the only choice for measuring it is by combining connecting images taken by the cameras, however, due to poor camera settings and lighting conditions, the images taken by camera 2 where the only ones which had sufficient quality to do so. For the visual inspection, as the process of counting the number of broken wires (NBW) was tedious, and the sheer amount of NBW large, the number of locations with broken wires (LBW) was counted instead. Only the part of the wire which had been bent was counted, which resulted in 5.2 m long piece of wire. This piece of wire was further cut in two because of practical reasons, just outside of the middle of the double-bending zone, resulting in one shorter half and one longer half. Which strands which originally was connected in the shorter- and longer halves was not kept a record of, as a result, the total number of LBW in each strand is unknown. The number of LBW in each layer of the SWR is presented graphically in Figure 5.7, and numerically together with the counter number of ruptured strands, in Table 5.3. These results should be used with caution, as, once again, the process was tedious, and the wires covered in grease, thus, prone to human error. Notice in Table 5.3 that a total of 10 strands where completely ruptured, however, none of them

are located in the outer layer, thus, through a manual inspection without picking the rope apart, they could not be found. This is interesting when considering that the [5, p. 19] recommends discarding a rope immediately if only one strand is completely ruptured, and at the same time recommends visual inspection as the assessment method for fractured strand(s) [5, p. 11]. For clarification purposes, a fractured strand corresponds to completely ruptured strand. One may be attempted to conclude that the 10 (counted) ruptured strands correspond to the ten events with energy larger than 5100 J shown in Figure 5.2, however, without further testing, this remains a topic of speculation.

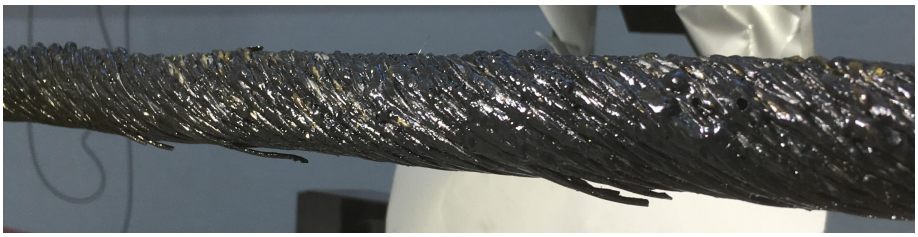

Figure 5.1: A picture of the SWR tested in the first test taken after it had been discarded. As seen in this figure, several broken wires are visible on the SWR

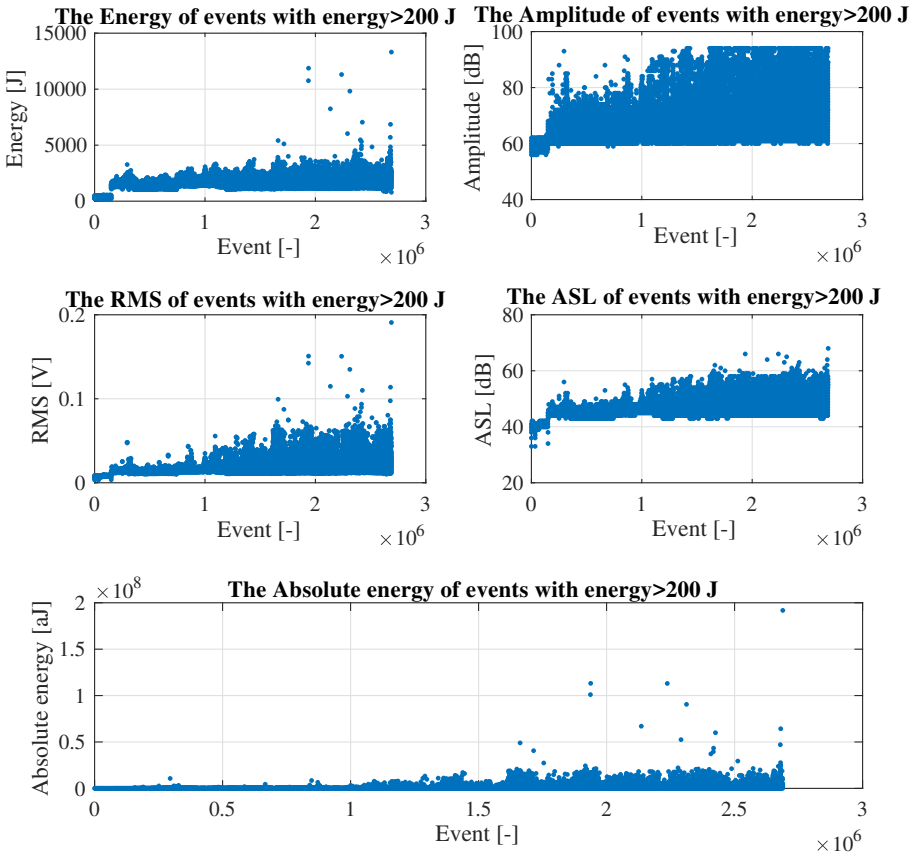

Figure 5.2: The AE variables of the first test which had a characteristic pattern through the fatigue life of the SWR, plotted against event number

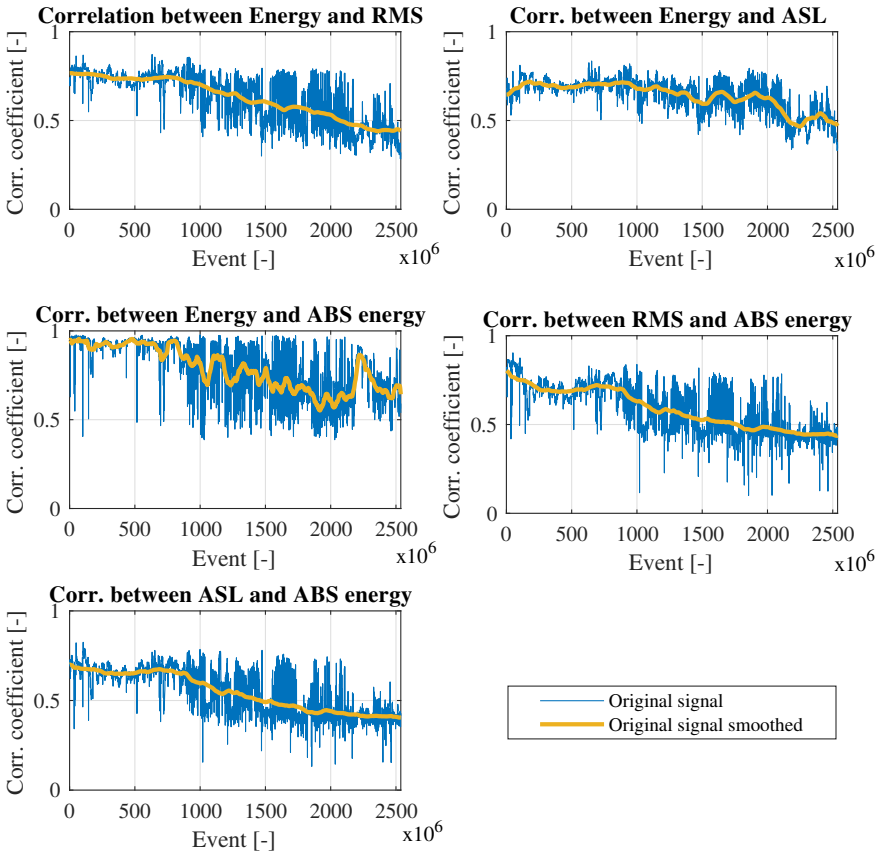

Figure 5.3: Correlation trends of the AE variables of the first test which had a characteristic pattern through the fatigue life of the SWR, i.e. the trends which also had a characteristic pattern through the fatigue life of the SWR, plotted against event number

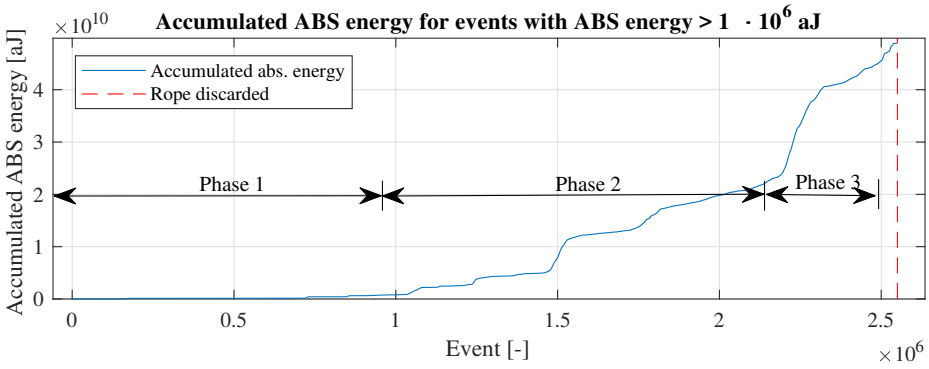

Figure 5.4: The accumulated ABS energy for events of the first test with ABS energy $1 \cdot 10^6\ aJ$

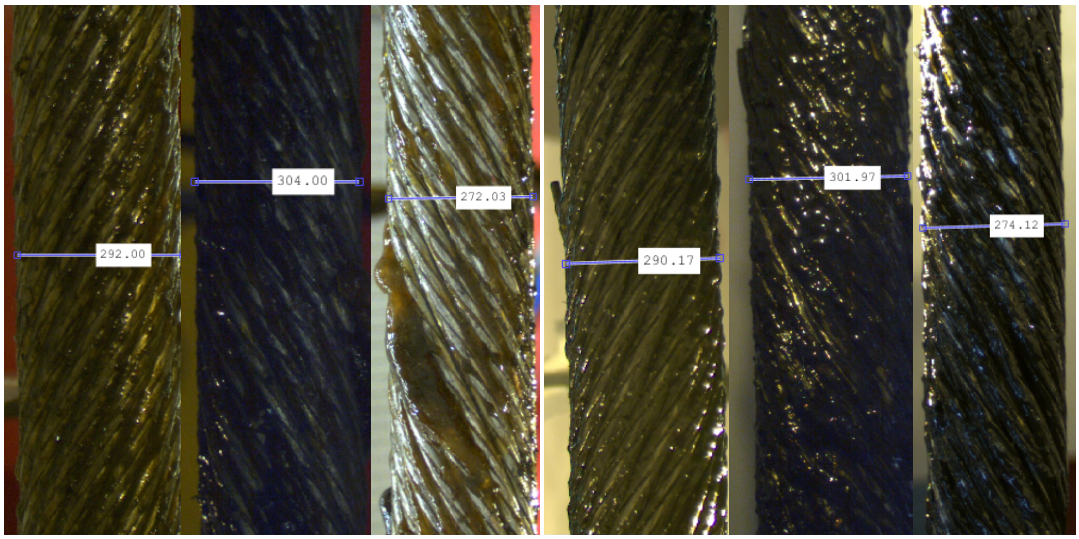

(a) Camera 1, cycle 1,000 (b) Camera 2, cycle 1,000 (c) Camera 3, cycle 1,000 (d) Camera 1, cycle 79,000 (e) Camera 2, cycle 79,000 (f) Camera 3, cycle 79,000

Figure 5.5: Diameter measurements using images taken by the camera system in the first test, for images taken at cycle 1,000 and 79,000, by all cameras. All lengths are in unit *pixel*. The results are summarised in Table 5.1. All images are taken in the double-bending zone, at approximately the same location

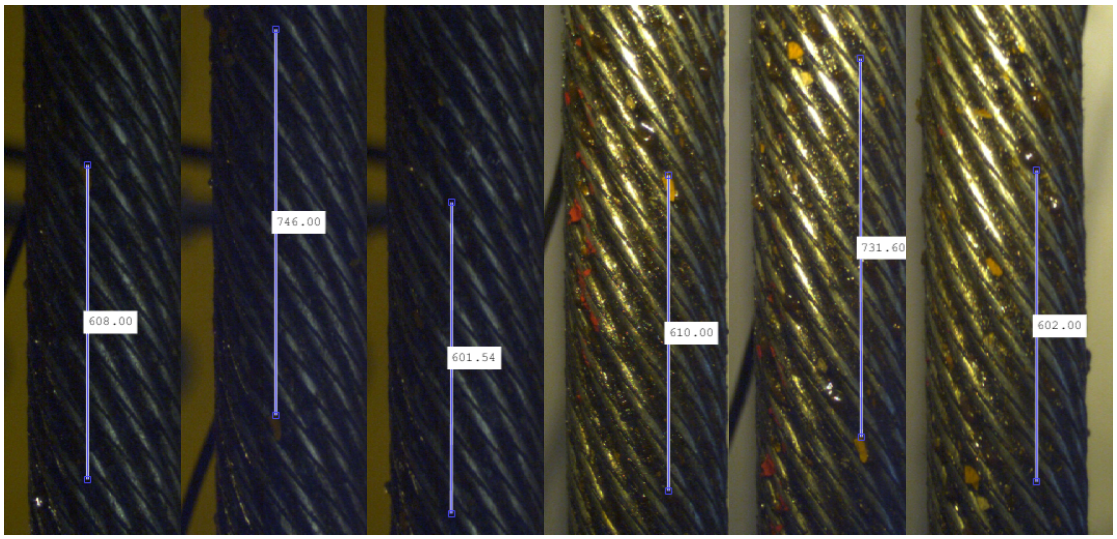

(a) Camera 2, cycle 1,000 (b) Camera 2, cycle 1,000 (c) Camera 2, cycle 1,000 (d) Camera 2, cycle 79,000 (e) Camera 2, cycle 79,000 (f) Camera 2, cycle 79,000

Figure 5.6: Lay length measurements using images taken by the camera system in the first test, for images taken at cycle 1,000 and 79,000, by camera 1. All lengths are in unit *pixel*. Figure 5.6a and 5.6d shows the axial length of the five first strands, Figure 5.6b and 5.6e the axial length of the six following strands, and Figure 5.6c and 5.6f shows the axial length of the five following and final strands. These measurements are the axial length of 16 strands, which is the number of strands in the outer layer, thus, the actual lay length is calculated by adding the lengths displayed in Figure 5.6a, 5.6b and 5.6c, and 5.6d, 5.6e and 5.6f, respectively. The results are summarised in Table 5.2. All images are taken in the non-bending zone, at the same location

Cycle	Measured diameter in pixels		
	Camera 1	Camera 2	Camera 3
1,000	292.00	304	272.03
79,000	290.17	301.97	274.12
Change	-1.83	-2.03	2.09

Table 5.1: Comparison of a selection of diameter measurements of the recordings by the camera system in the first test. All lengths are in unit *pixel*. The measurements are presented graphically in Figure 5.5

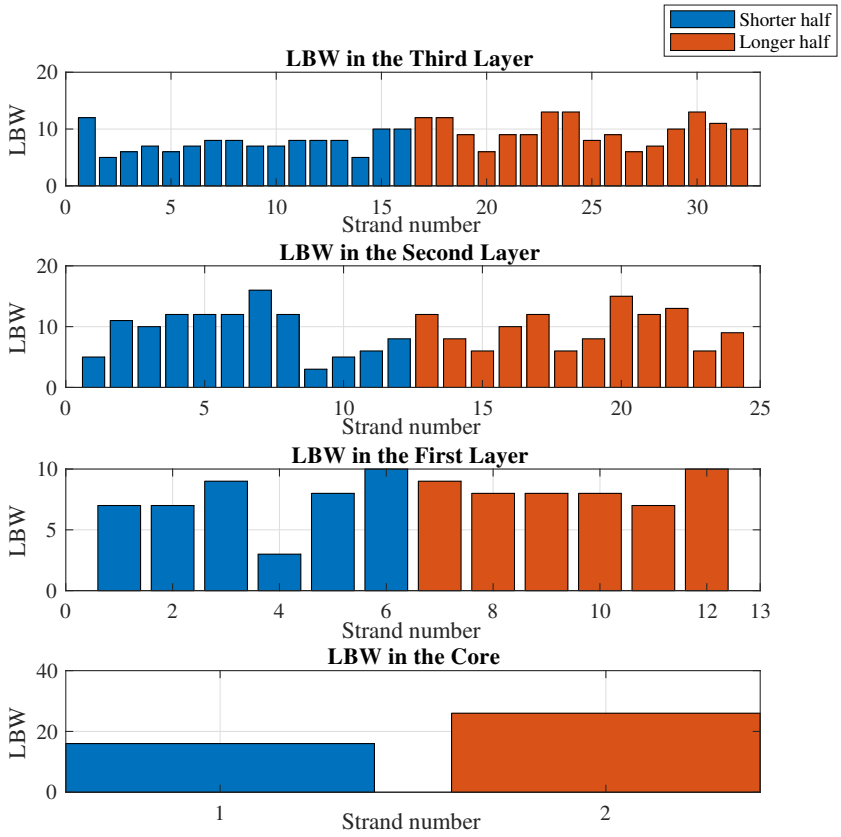

Figure 5.7: The counted number of LBW in each layer of the wire

Cycle	Lay length
1,000	$608 + 746 + 601.54 = 1955.54$
79,000	$610 + 731.60 + 602 = 1943.60$
Difference	-11.94, $(1943.60 - 1955.54)/1955.54 = -0.61\%$

Table 5.2: Lay length measurements of the first test, all measurements are based on the videos recorded by the same camera, which are displayed in Figure 5.6, and have unit *pixel*

Location	Ruptured strands	LBW	Average LBW per strand
3rd layer	0	279	$279/16 \approx 17.4$
2nd layer	4	229	$229/12 \approx 19.1$
1st layer	4	94	$94/6 \approx 15.7$
Core	2	42	$42/1 = 42$
Sum	10	644	

Table 5.3: The counted number of wires and strands in each layer of the SWE tested in the first test. The 1st layer is surrounding the core, the 2nd layer is surrounding the 1st layer, and the 3rd layer is the outer layer and surrounds the 2nd layer

5.2 Second test

The rope endured 115,574 cycles before a rapid, and almost total rupture occurred, as seen in Figure 5.8. The recorded and filtered AE data are presented in Figure 5.9 and a selection of magnetic measurements are shown in Figure 5.10. As diameter measurements were unsuccessful in the first test, they are not repeated in later tests. Due to poor camera settings and lighting conditions, which additionally were worsened by the water on the SWR from the static AE interface, it was impossible to perform lay length measurements. As seen in the AE data it appears that the 2nd channel somehow lost its signal at sample $5.5 \cdot 10^6$, further, although channel 1 and 2 have several significant fluctuations in voltage, neither of them shows any apparent signs of deterioration. Hence, the AE measurements aren't furthered processed. Figure 5.10 displays the raw measurements of the magnetic tester at four different cycles, notice the exponential increase in amplitude between the measurements of the later cycles. Figure 5.11 shows the processed magnetic measurements from the same test, i.e. the highest absolute amplitude-, the RMS-, and the integrated amplitude of each measurements as a function of cycle. As seen in the latter figure, the highest amplitude as a function of cycle reveals a sharp increase in amplitude at cycle 105,000 before the SWR ruptured. While the RMS as a function of cycle reveals deterioration already at cycle 60,000. The integrated amplitude as a function of cycle does not seem to reveal any information about deterioration which the highest- or integrated amplitude as a function of cycle has not announced in advance, with the exception of amplitude of the second coil being generally larger than that of the first coil. As opposed to the wires tested in the first, third and fourth test, not a lot of oil was released from the wire during the test, possibly because the oil's viscosity is increased as results of the cooling from the water. The water had a temperature of 9.2 ^oC and the SWR around the traction sheave, which is defined in Figure 3.1, had a maximum temperature of 32 ^oC, which is higher than the maximal temperature of the SWR just outside the test sheave, which had a maximal temperature of 27.2 ^oC as presented in Figure 4.6a. Thus, confirming the cooling effects of the water supplied by the AE static interface, as the rope temperature is expected to be higher at the test sheave than on the traction sheave.

Figure 5.8: A picture of the second rope tested in this thesis subsequent to failure, the rope experienced a rapid and almost total rupture. Prior to this, the measurements of the magnetics tested revealed an exponentially increasing discontinuity, yet the outside of the rope didn't show any obvious signs of such a massive deterioration

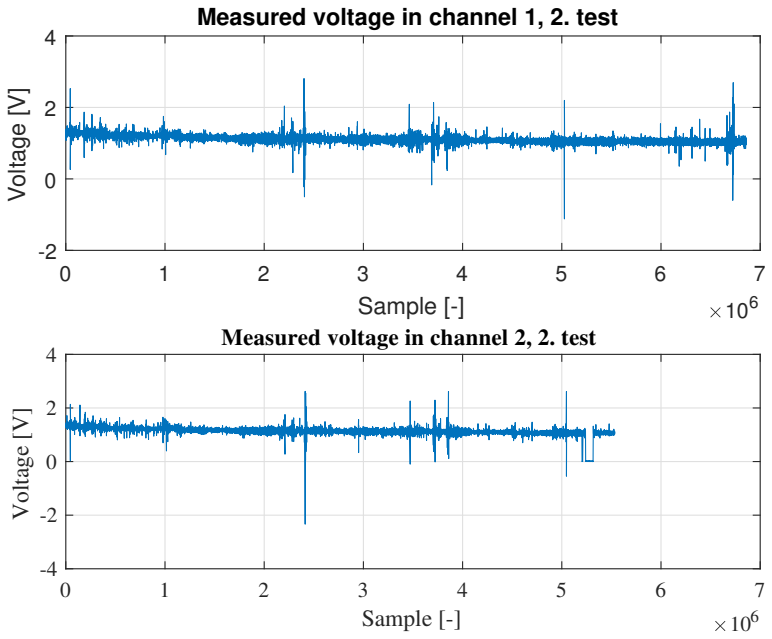

Figure 5.9: The recorded and filtered AE data of the second test

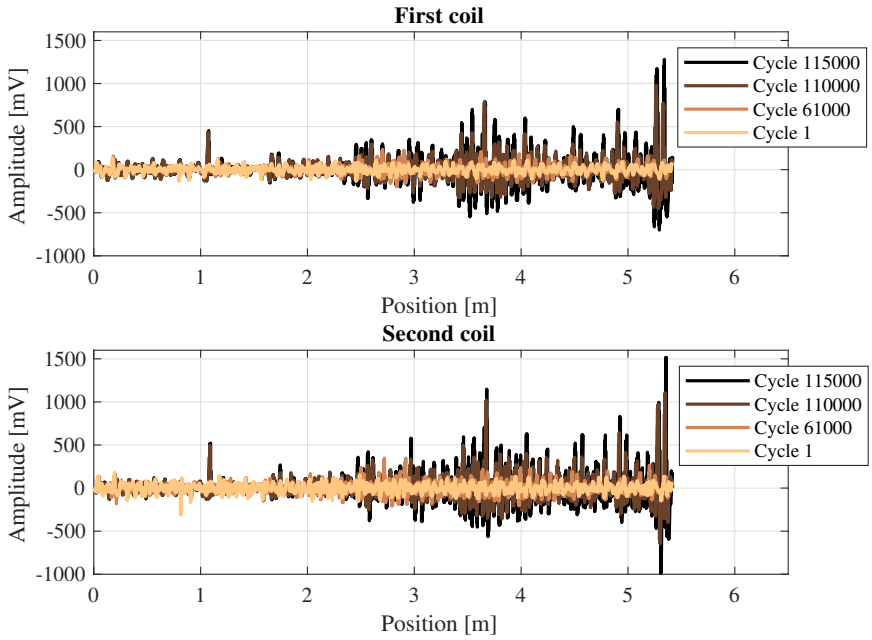

Figure 5.10: The raw measurements of the magnetics tester of the second test, shown at a selected number of cycles

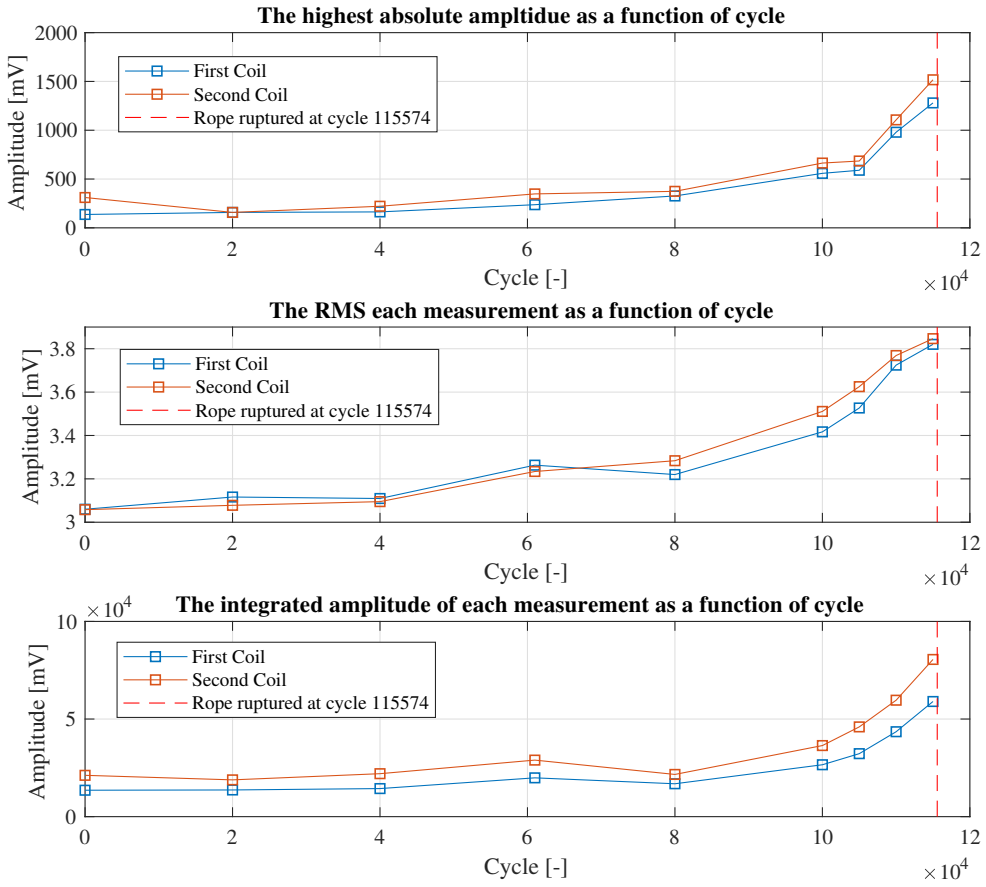

Figure 5.11: The processed magnetic measurements of the second test

5.3 Third test

The rope endured 115,216 cycles before the discard criterion was met. At the time the SWR was discarded, it looked very much like the SWR of the first test, as shown in Figure 5.1. The AE measurements are presented in Figure 5.12, as these measurements nor indicate deterioration or seem physically realistic, one or more technical errors are believed to be present in the custom AE sensor system. Hence, the AE measurements are once again not furthered processed. Similarly to the second test, Figure 5.13 displays the raw measurements of the magnetic tester at four different cycles, which once again shows an exponential increase in amplitude between the measurements of the later cycles. Figure 5.14 shows the processed magnetic measurements from the same test, i.e. the highest absolute amplitude-, the RMS-, and the integrated amplitude of each measurements as a function of cycle. As seen in the latter figure, the highest amplitude as a function of cycle reveals a sharp increase in amplitude at cycle 81,300. While the RMS as a function of cycle reveals deterioration already at cycle 28,100. Once again, the integrated amplitude as a function of cycle does not seem to reveal any information about deterioration which the highest- or integrated amplitude as a function of cycle has not announced in advance, with the exception of amplitude of the second coil being generally larger than that of the first coil. One may raise the question why there were not conducted more

measurements with the magnetic tester before rope failure. The reason for this is that the doubt was raised towards our discard criterion as the SWR of the second test ruptured, thus, damaging the magnetic tester. As the magnitude of the magnetic measurements of the third test was closing up on the ones from the second test, to be on the safe side, a decision was made to unmount the magnetic tester before the SWR is discarded. In hindsight, the discard criterion resulted in a ruptured SWR only in the second test. Additionally, the magnetic measurements of the 24 and 26 mm SWR aren't directly comparable as they are conducted with coils of different size, as described in Section 3.2. Hence, a better decision would be not to unmount the magnetic tester. Lay lengths measurements based on data from the camera system are presented graphically in Figure 5.15, additionally, they are summarised in Table 5.4. Similar to the lay length measurements of the first test, the results of the third test show that the lay length is decreasing.

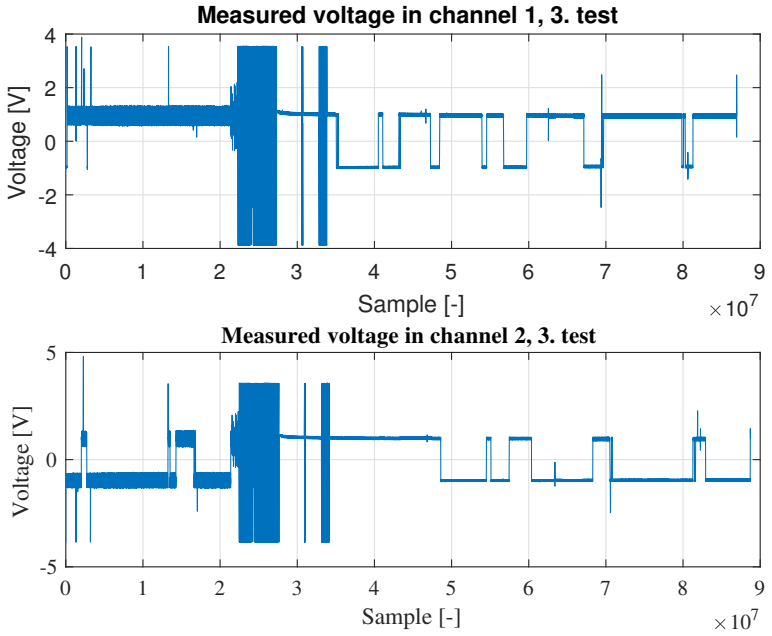

Figure 5.12: The recorded and filtered AE data of the third test

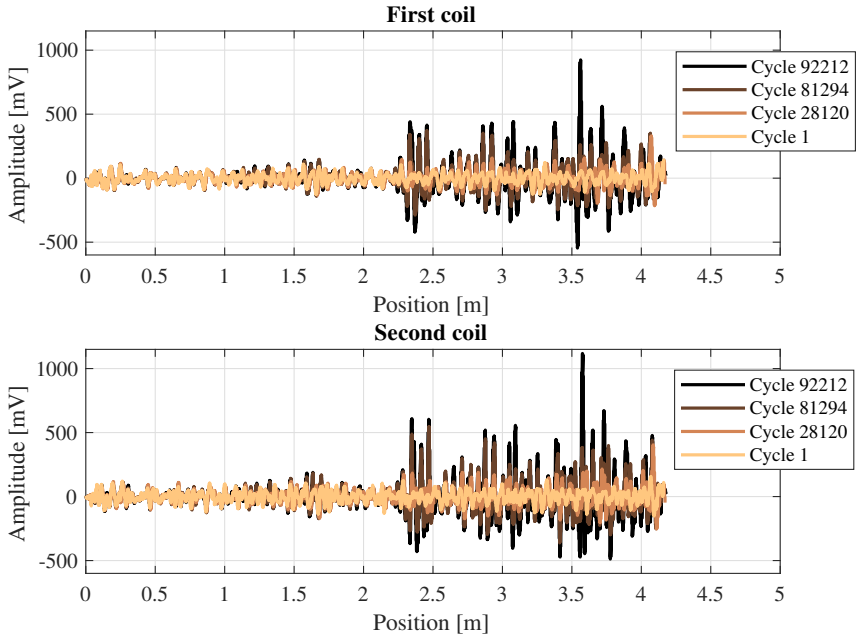

Figure 5.13: The measurements of the magnetics tester conducted in the third test

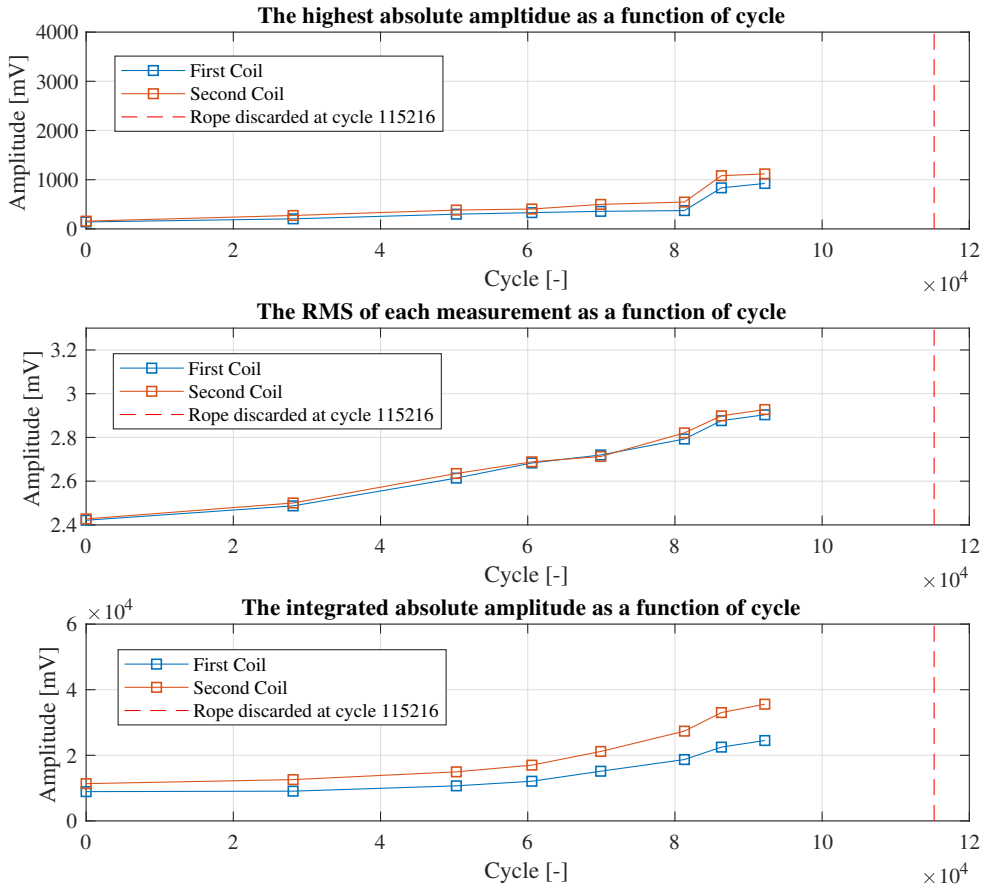

Figure 5.14: The processed magnetic measurements of the third test

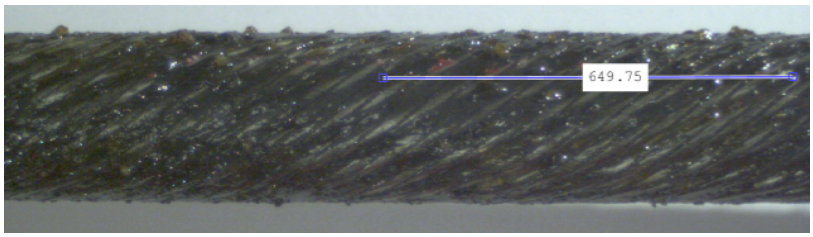

(a) Camera 3, cycle 1,000

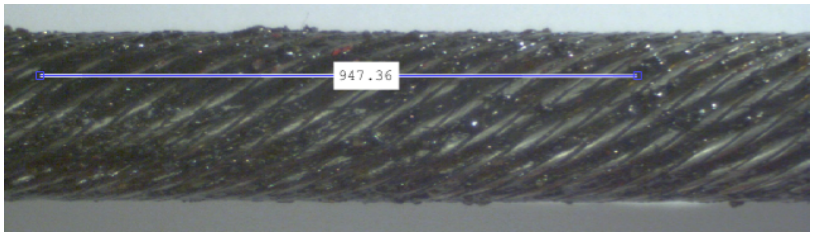

(b) Camera 3, cycle 1,000

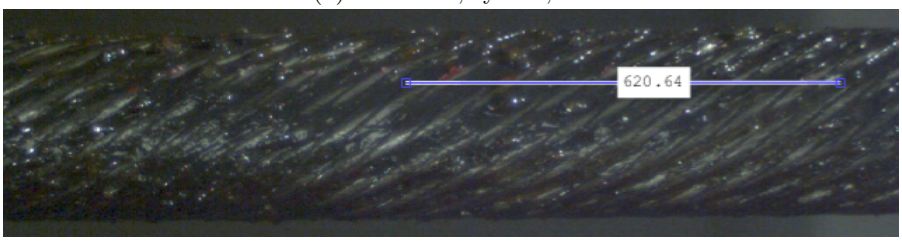

(c) Camera 3, cycle 114,000

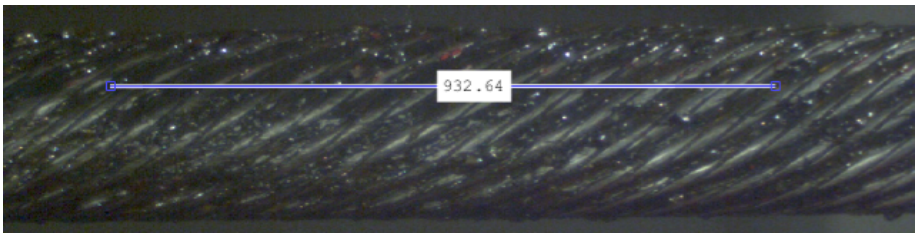

(d) Camera 3, cycle 114,000

Figure 5.15: Lay length measurements using images taken by the camera system in the third test, for images taken at cycle 1,000 and 114,000, by camera 3. All lengths are in unit *pixel*. Figure 5.15a and 5.15c shows the axial length of the seven first strands, Figure 5.15b and 5.15d the axial length of the nine following strands. These measurements are the axial length of 16 strands, which is the number of strands in the outer layer, thus, the actual lay length is calculated by adding the lengths displayed in Figure 5.15a and 5.15b, and 5.15c and 5.15d, respectively. The results are summarised in Table 5.4. All images are taken in the non-bending zone, at the same location.

Cycle	Lay length
1,000	649.75+947.36=1597.11
114,000	620.64+932.64=1553.28
Difference	-43.83, $(1553.28 - 1597.11)/1597.11 = -2.7\%$

Table 5.4: Lay length measurements of the third test, all measurements are based on the videos recorded by the same camera, which are displayed in Figure 5.15, and have unit *pixel*.

5.4 Fourth test

The rope endured 117,638 cycles before the discard criterion was met. Similarly to the SWR of the third test, at the time the SWR of the fourth test was discarded, it looked very much like SWR of the first test, as shown in Figure 5.1. Initially, the sensor was positioned on the sheave, however, as the corresponding AE measurements which are presented in Figure 5.16a shows, our system seems to be too sensitive for such a sensor position, as noise at this position has high intensity throughout the entire measurement range. Hence, the AE sensor was re-positioned at the wire, similar to the 1st and 3rd test, with corresponding measurements presented in Figure 5.16b. As seen in this figure in the measurements of channel 1, several of the major fluctuations occur at later samples, however, similar to the AE data of the second test, the measurements in both channels do not show any obvious signs of deterioration. Hence, similar to the second and third test, they aren't furthered processed. As mentioned in Section 3.3.2, the custom AE sensor system is designed in such a way that the polarity of the two voltage channels may change under a recording. This polarity switching is particularly visible in the measured voltage in channel 2 shown in Figure 5.16b. Additionally, the measurement range of the custom AE sensor system seems to be too small for this sensor position. Similarly to the second and third test, Figure 5.17 displays the raw measurements of the magnetic tester at four different cycles, which once again shows an exponential increase in amplitude between the measurements of the later cycles. Figure 5.11 shows the processed magnetic measurements from the same test, i.e. the highest absolute amplitude-, the RMS-, and the integrated amplitude of each measurements as a function of cycle. As seen in the latter figure, the highest amplitude as a function of cycle reveals a sharp increase in amplitude at cycle 102,000 before the SWR is discarded. The RMS- and integrated amplitude as a function of cycle reveals deterioration already at cycle 51,000 and that the amplitude of the second coil is generally larger than that of the first coil. Lay length measurements based on data from the camera system are presented graphically in Figure 5.19, additionally, the results are summarised in Table 5.5.

As the lay length measurements of different tests are based on different cameras or camera positions, only the relative changes in lay length for the different tests should be compared. Similar to the lay length measurements of the first and third test, the results for the fourth test shows that the lay length has decreased. The author must admit he finds the decrease in lay length counter intuitive, and a physical explanation on how this can be remains absent. In future tests it would be interesting to see if the decrease in lay length also occurs in the bending zone of the SWR.

One might ask the question on how the SWR tested in the third and fourth test endured $(115,216 - 79,866)/79,866 = 44\%$ $(117,638 - 79,866)/79,866 = 47\%$ more cycles than the SWR tested in the first test, respectively, with identical test conditions. One plausible explanation is that in each test, oil from the tested SWR was transferred to the test sheave, and as this sheave wasn't cleaned in between tests, the third- and especially the fourth SWR tested, were much more lubricated than the first SWR tested. It is emphasised that the SWR tested in the first-, third- and fourth test all originated from the same SWR. By considering that the SWR in the second test ruptured and the SWR of in first-, third- and fourth test did not, our discard criterion may have potential for improvement. However, as CM is the primary interest of these tests, and not fatigue of SWR, the discard criterion is not further addressed.

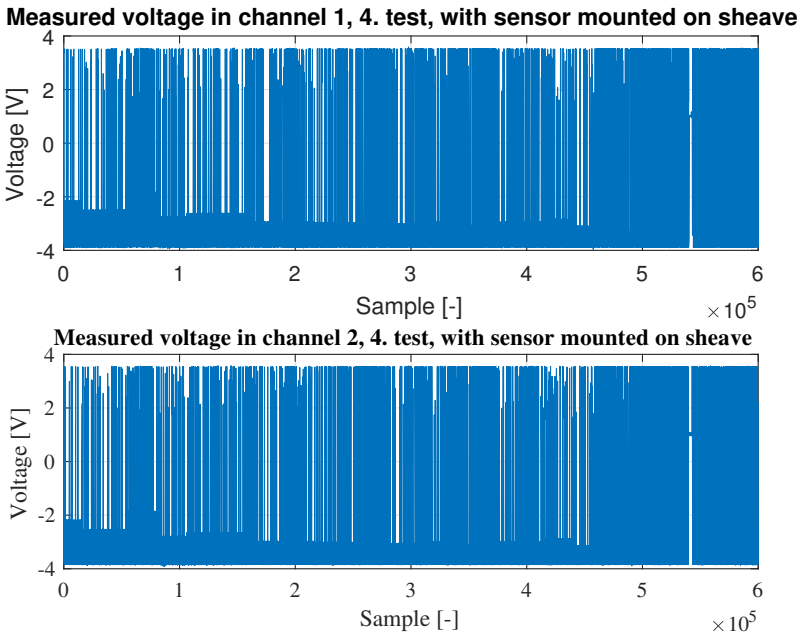

(a) The AE measurements with corresponding sensor mounted on the test sheave

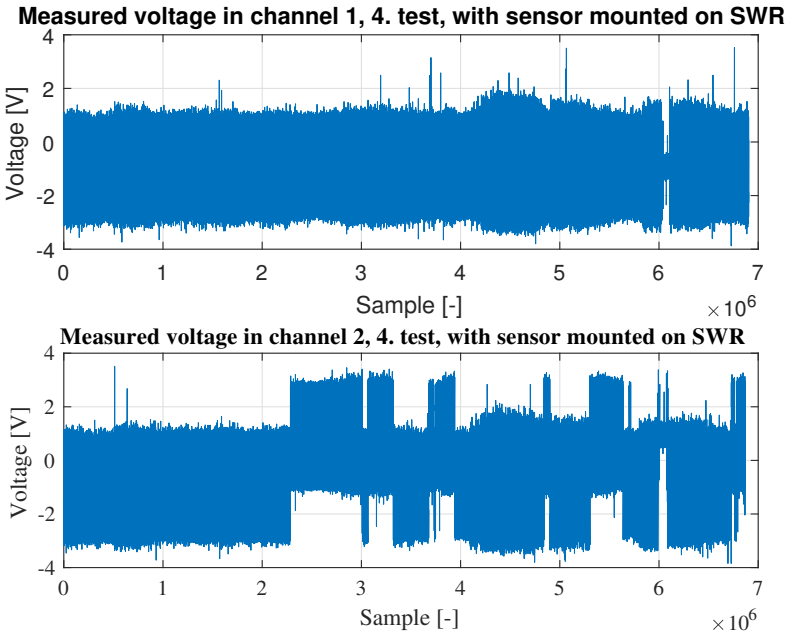

(b) The AE measurements with corresponding sensor mounted on the SWR

Figure 5.16: The recorded and filtered AE data of the fourth test

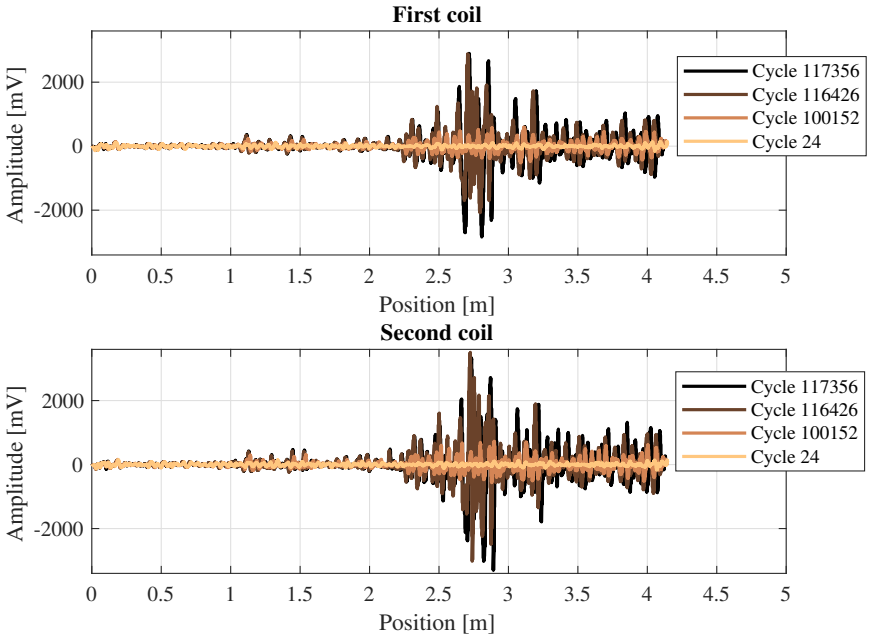

Figure 5.17: The raw magnetic measurements of the fourth test

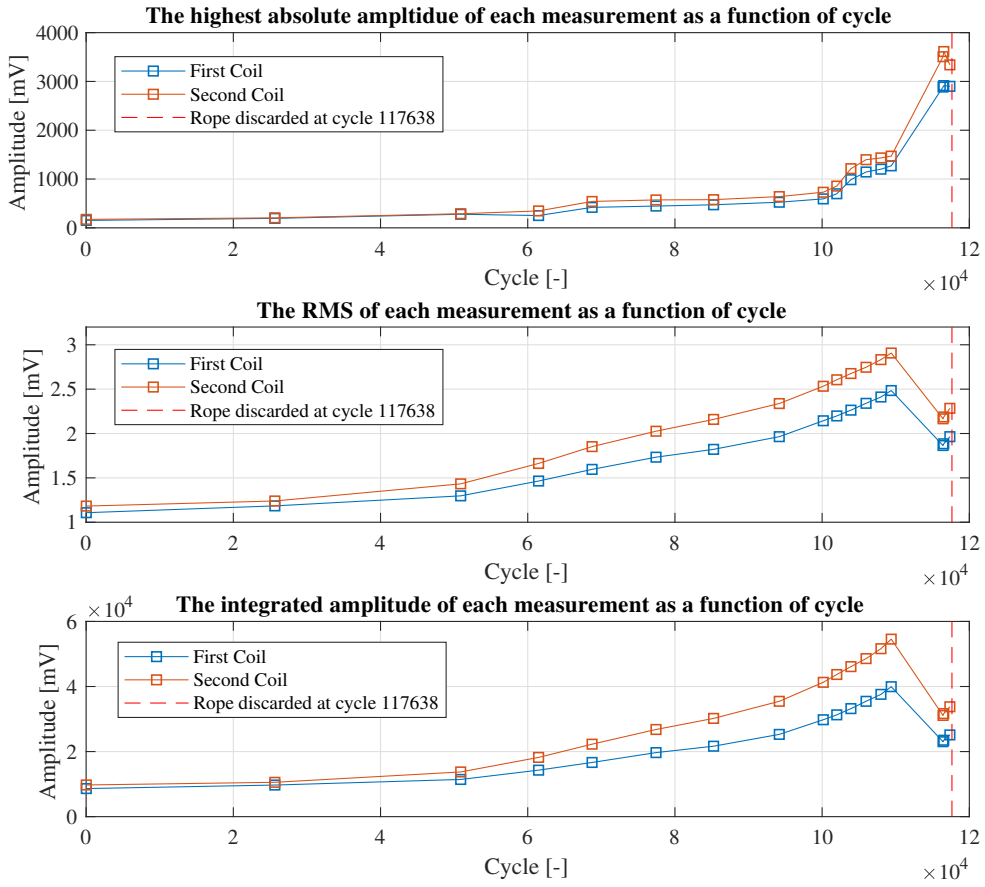

Figure 5.18: The processed magnetic measurements of the fourth test

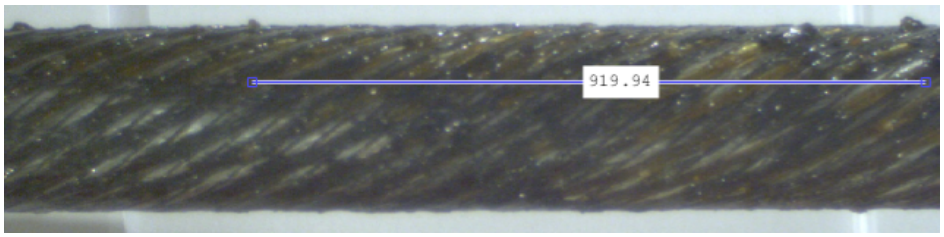

(a) Camera 2, cycle 1350

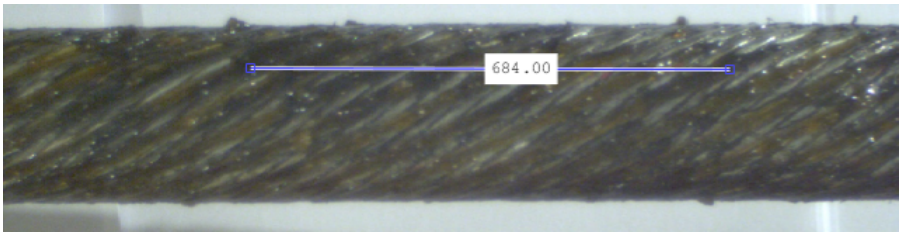

(b) Camera 2, cycle 1350

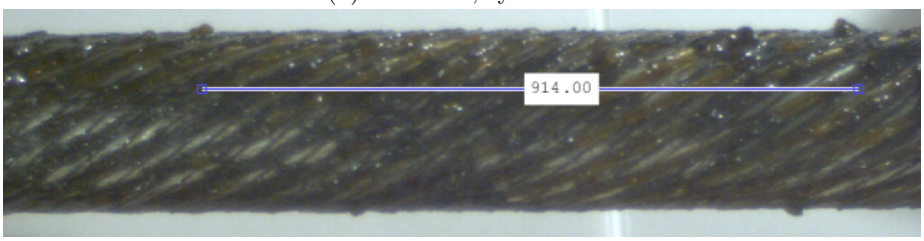

(c) Camera 2, cycle 117336

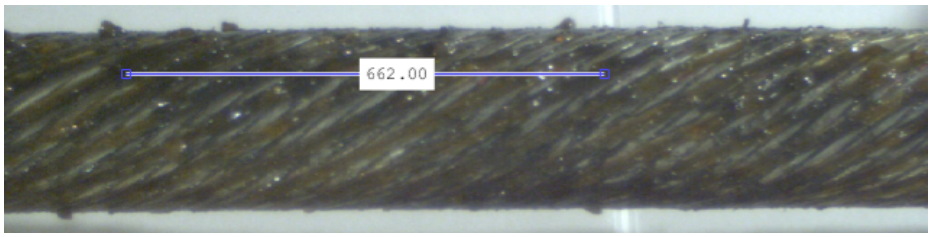

(d) Camera 2, cycle 117336

Figure 5.19: Lay length measurements using images taken by the camera system in the fourth test, for images taken at cycle 1350 and 117336, by camera 2. All lengths are in unit *pixel*. Figure 5.19a and 5.19c shows the axial length of the nine first strands, Figure 5.19b and 5.19d the axial length of the seven following strands. These measurements are the axial length of 16 strands, which is the number of strands in the outer layer, thus, the actual lay length is calculated by adding the lengths displayed in Figure 5.19a and 5.19b, and 5.19c and 5.19d, respectively. The results are summarised in Table 5.5. All images are taken in the non-bending zone, at the same location

Cycle	Lay length
1350	919.94+684=1603.4
117336	914+662=1576
Difference	-27.4, (1576-1603.4)/1603.4=-1.7%

Table 5.5: Lay length measurements of the fourth test, all measurements are based on the videos recorded by the same camera, which are displayed in Figure 5.19, and have unit *pixel*

Chapter 6

Conclusions and Recommendations

Several measurable quantities and features that indicate deterioration of the SWR during a simple bending test were identified in this thesis.

Starting with measurements of the MISTRAS AE sensor system, the energy, amplitude, RMS, ASL, and ABS energy was found to indicate deterioration, as was also the case for the correlation between energy and RMS, energy and ASL, energy and ABS energy, RMS and ABS energy, and ASL and ABS energy. Additionally, the perhaps most noteworthy discovery is the accumulated ABS energy as a function of the event, which revealed that the SWR experience the typical three-phase fatigue process. The measurements of the custom AE sensors did not show deterioration in any of the tests, for any sensor placing, possibly due to one or more technical difficulties.

From the measurements of the magnetic tester, deterioration was easily identified from the raw measurements alone. By processing these measurements further, early signs of deterioration were found to be revealed by considering the RMS of each measurements as a function of cycle and in one test also the integrated amplitude as a function of cycle, while the highest amplitude as a function of cycle revealed the sharp exponential increase in deterioration prior to failure, which is believed to be highly valued in any industrial appliance of SWR. Thus, the measurements of the magnetics tester recognises the three-phase fatigue process of SWR in simple bending tests, which in this thesis is identified in the measurements of the MISTRAS AE sensor system.

The camera system was able to detect changes in lay length in the non-bending zone between the first measurement conducted after the initial settling, and last measurements conducted before the rope was discarded. The relative differences were distinct for every test, even though the SWR and test conditions were identical in the first, third and fourth test. Further, the camera system was unable to detect changes in the diameter of SWR, as the measurement error is believed to be higher than the actual difference.

6.1 Recommendations

For future tests using a camera system to detect deterioration of a SWR, the author recommends including a ruler scale in the cameras image area, thus, allowing for consistent calibration of images. To quickly identify the same location on the SWR in different video recordings, it is recommended to create a landmark on the SWR, i.e. a recognisable location which stays constant throughout the test, possibly by the use of paint. A final recommendation on the use of a camera system, if it is intended to be used to measure changes in SWR diameter, would be to fill a large part of the image area with the width of SWR, thus, having the maximum amount of pixels per SWR width. The resulting increased resolution should, in principle, make it easier to detect small changes in SWR diameter.

6.2 Future work

Much work remains before a CM model can be created based on the measurements obtained by the CM technologies utilised in this thesis. Based on measurements from the MISTRAS AE sensor system and magnetics tester, the fatigue process of SWR is three-faced. Lay length measurements should be performed in the bending zone of the SWR, and results compared with the non bending zone. Further, by automating the lay length measurements, or by conducting a series of manual measurements, the trends of lay length as a function of cycle can be explored. Thus, revealing whether or not it indicates deterioration. Besides collecting more data with the CM technologies in future fatigue test of SWR, the next step in creating the CM model is either by constructing a new, or modify an existing, three-phase fatigue model to the measurements of the magnetic tester and MISTRAS AE sensor system.

Bibliography

[1] K. Feyrer, (2015). *Wire ropes: tension, endurance, reliability.* Springer, 2017. p. 220: Elements which have influence on fatigue life of SWRs.

[2] Alioto Group, *Most important discard criteria*, n.d.. Accessible from: http://www.aliotogroup.com/wp-content/uploads/2014/02/principali-criteri-scarto.pdf (Picked up: 22. Jan. 2018)

[3] R. Schlanbusch, E. Oland and E. Bechhoefer, "Condition monitoring technologies for steel wire ropes - A review," *International Journal of Prognostics and Health Management*, vol. 8, nr. 1, Jan., 2017. ISSN: 2153-2648.

[4] D.Elata, R.Eshkenazy, M.P.Weiss, "The mechanical behavior of a wire rope with an independent wire rope core", *International Journal of Solids and Structures*, vol. 41, nr. 5-6, pp. 1157-1172, Mar., 2004. DOI:$https://doi.org/10.1016/j.ijsolstr.2003.11.021$.

[5] *Cranes — Wire ropes — Care and maintenance, inspection and discard*, ISO 4309, 2010.

[6] P. T. Gibson, F. G. White, L. A. Schalit, R. E. Thomas, R. W. Cote, and H. A. Cress, "A STUDY OF PARAMETERS THAT INFLUENCE WIRE-ROPE FATIGUE LIFE," BATTELLE Columbus Laboratories Long Beach Research Facility, California, United States of America, (no report number),31. Oct., 1974.

[7] C.R.Chaplin, "Failure mechanisms in wire ropes," *Engineering Failure Analysis*, vol. 2, nr. 1, pp. 45-57, Mar., 1995. DOI: 10.1016/1350-6307(95)00004-A.

[8] R. Woernle, "Ein Beitrag zur Klärung der Drahtseilfrage," *Z. VDI*, vol. 72, nr. 13, pp. 417–426, 1929.

[9] J. Hankus, "Fatigue tests on hoisting wire ropes of diameters above 50 mm," OIPEEC Round Table, East Kilbride Glascow, Scotland, Jun. 1985.

[10] N. A. Fleck, C. S. Shin, R.A. Smith, "Fatigue Crack Growth Under Compressive Loading," *Engineering Fracture Mechanics*, vol. 21, nr. 1, pp. 173–185, 1985. DOI: 10.1016/0013-7944(85)90063-3.

[11] K. Feyrer, "Die Biegewechselzahl von Standardseilen beim Einfachbiegeversuch", *DRAHT*, vol. 32, nr. 10, 1981, p. 556–558 and nr. 11, pp. 603–606.

[12] K. Feyrer, "Effect of bending length on endurance of wire ropes," *Wire World*, vol. 23, pp. 115–119, 1981.

[13] D.G Shitkow, I.T. Pospechow, *Drahtseile*. Berlin: VEB Verlag Technik, 1957.

[14] K. Feyrer, W. Vogel, "High-strength fibre rope running over rope pulleys," *WIRE*, vol. 42, nr.5, pp. 455–458, 1992, and *DRAHT*, vol. 42, nr. 11, 1991.

[15] H. Müller, "Drahtseile im Kranbau," *VDI-Bericht*, nr. 98, and *dhf*, vol. 12, nr. 11, pp. 714–716, 1966 and vol. 12, pp. 766–773.

[16] E. Wolf, "Seilbedingte Einflüsse auf die Lebensdauer laufender," *DRAHT*, vol. 39, nr. 11, pp. 1088–1093, 1988.

[17] K. Feyrer, "The Service Lives of Running Wire Ropes under the Influences of Size Effect," *Lift Report*, vol. 31, nr. 1, pp. 20-26, 2011.

[18] H. Müller, "The properties of wire rope under alternating stresses," *Wire World*, vol. 3, nr. 5, pp. 249–258, 1961.

[19] B. Bertsche, G. Lechner, *Zuverlässigkeit im Maschinenbau*, New York: Springer-Verlag Berlin, 1990.

[20] P.D.T O'Connor, *Zuverlässigkeitstechnik*, Weinheim: VCH Verlagsgesellschaft mbH, 1990.

[21] P. Greis, "Untersuchung der Lebensdauer von Drähten und Seilen für Krananlagen," *Stahl Eisen*, vol. 99, nr. 10, pp. 518–527, 1979.

[22] Magnet Rope Testing, University of Stuttgart, Stuttgart, Baden-Württemberg, Germany, 2013.

[23] N.F.Casey, P.A.A.Laura, "A review of the acoustic-emission monitoring of wire rope," *Ocean Engineering*, vol. 24, nr. 10, 9. May, pp. 935-947, 1997. DOI: https://doi.org/10.1016/S0029-8018(96)00052-2.

[24] Electronics Tutorials, *Passive Band Pass Filter*, n.d.. Accessible from: https://www.electronics-tutorials.ws/filter/filter_4.html. Picked up: 13. Feb., 2018.

[25] M. Rudermann, "Digital Control," n.d.. (Powerpoint, course: MAS508, University of Agder)

[26] R. Schlanbusch, E. Bechhoefer, T. J. J. Meyer. "Low Computation Acoustic Emissions Structural Health Monitoring Through Analog Signal Pre-Processing". *Annual Conference of the Prognostics and Health Management Society 2017* (August 2017). Accessed at 20.4.2017 through: *https://www.phmsociety.org/node/2305*

[27] T.S. Golosinski, A. Tytko (1998). "Magnetic examination of wire ropes: loss of metallic area (LMA) measurement with Hall effect sensors". *OIPEEC Bulletin* No. 75 23 37 ISSN 1018-8819

[28] E. S. Wacker, J. Denzler. *Enhanced anomaly detection in wire ropes by combining structure and appearance.* Pattern Recogn. Lett. 34, 8 (June 2013), 942-953. DOI=http://dx.doi.org/10.1016/j.patrec.2013.01.025

[29] OIPEEC,"OIPEEC Recommendation No. 4", *Bulletin*, vol. 56, 1988.

[30] *Standard Terminology for Nondestructive Testing*, ASTM E1316 - 05, 2005.

[31] MISTRAS, *AEwin^{TM} Software User's manual Rev 4*, October 2014.

Appendix

Contents of Appendix

A: Data sheet for the 26 mm SWR test in this thesis

1. Offer Reference:	
Customer reference:	26mm Low Rotation Crane Wire
Certex reference:	TBA
Application :	Multilayer spooled Crane or Winch Rope

2. Rope Description	
Rope type:	Bridon Dyform 34LR
Rope Construction:	Dyform 34 x7 LR (16/6&6/6/1) Right hand langs lay (zZ)

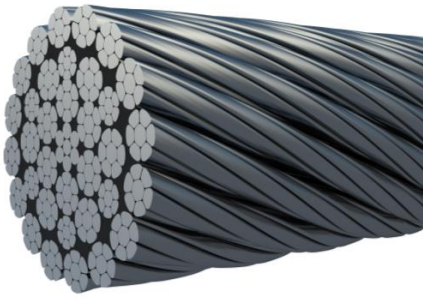

3. Dimensions		
Rope nominal diameter:	d	26mm
Rope diameter tolerance:	d_{max}, d_{min}	+2% to +4%
Rope nominal length:	L	TBA
Rope length tolerance:	$L_{max}L_{min}$	+0 +1%

4. Strength		
Wire tensile strength (grade):	*UTS*	1960 N/mm^2
Nominal metallic area:	A	394 mm^2
Minimum breaking force:	F_m	63.5 tonnes

5. Additional Property Information		
Nominal rope length mass in air:	m	3.46 kg/m
Nominal rope length mass in seawater:	m_s	
Nominal total mass (nett weight) in air:		
Nominal rope axial stiffness @ 20% MBL:	EA	39 MN
E Modulus @ 20%	E	99 kN/mm^2
Nominal torque factor @ 20% MBL:	C_γ	1.8 %
Nominal turn factor @20% MBL:	C_ϑ	0.7 °/m
Wire finish:		Drawn Galvanised
Lubrication (operating temperature):		Brilube 20 (-58°C to +110°C)
Packaging:	TBC	

6. Terminations	
Transport reel outboard end:	TBA
Transport reel inboard end:	TBA

B: Data sheet for the 24 mm SWR test in this thesis

1. Offer Reference:	
Customer reference:	24mm Low Rotation Crane Wire
Certex reference:	TBA
Application:	Multilayer spooled Crane Rope Rated Temperature -40°C

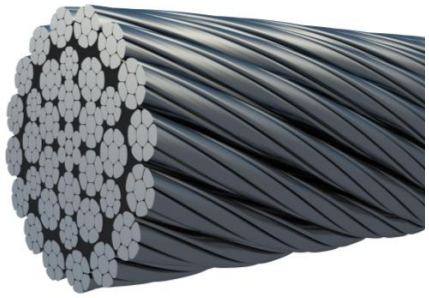

2. Rope Description	
Rope type:	Bridon Dyform 34LR
Rope Construction:	Dyform 34 x7 LR (16/6&6/6/1) Right hand langs lay (zZ)
Rope Specification:	EN 12385

3. Dimensions		
Rope nominal diameter:	d	24mm
Rope diameter tolerance:	d_{max}, d_{min}	+2% +4%
Rope nominal length:	L	TBA
Rope length tolerance:	$L_{max}L_{min}$	+0 +1%

4. Strength		
Wire tensile strength (grade):	UTS	1960 N/mm^2
Nominal metallic area:	A	334.0 mm^2
Minimum breaking force:	F_m	54.1 tonnes

5. Additional Property Information		
Nominal rope length mass in air:	m	2.93 kg/m
Nominal rope length mass in seawater:	m_s	2.58 kg/m
Nominal total mass (nett weight) in air:		TBA
Nominal rope axial stiffness @ 20% MBL:	EA	33.0 MN
E Modulus @ 20%	E	99 kN/mm^2
Nominal torque factor @ 20% MBL:	C_γ	1.8 %
Nominal turn factor @20% MBL:	C_ϑ	0.7 °/ rope lay
Wire finish:		Drawn Galvanised
Lubrication (operating temperature):		Brilube 20 (-58°C to +110°C)
Packaging:	TBA	

6. Terminations	
Transport reel outboard end:	TBA
Transport reel inboard end:	TBA